UNIVERSITÀ DI SIENA 1240

USiena

Selective Fatty Acid Amide Hydrolase Inhibitors as Potential Novel Antiepileptic Agents

This is the peer reviewed version of the following article:

Original:

Grillo, A., Fezza, F., Chemi, G., Colangeli, R., Brogi, S., Fazio, D., et al. (2021). Selective Fatty Acid Amide Hydrolase Inhibitors as Potential Novel Antiepileptic Agents. ACS CHEMICAL NEUROSCIENCE, 12(9), 1716-1736 [10.1021/acschemneuro.1c00192].

Availability:

This version is availablehttp://hdl.handle.net/11365/1146130 since 2021-09-21T18:27:50Z

Published:

DOI: http://doi.org/10.1021/acschemneuro.1c00192

Terms of use:

Open Access

The terms and conditions for the reuse of this version of the manuscript are specified in the publishing policy. Works made available under a Creative Commons license can be used according to the terms and conditions of said license.
For all terms of use and more information see the publisher's website.

(Article begins on next page)

07 October 2026

Selective Fatty Acid Amide Hydrolase Inhibitors as Potential, Novel Anti-Epileptic Agents

Alessandro Grillo,[§] Filomena Fezza,[¥] Giulia Chemi,[§,†] Roberto Colangeli,[£,♪] Simone Brogi,[¥] Domenico Fazio,[¶] Stefano Federico,[§] Alessandro Papa,[§] Nicola Relitti,[§,†] Roberto Di Maio,[$] Gianluca Giorgi,[§] Stefania Lamponi,[§] Massimo Valoti,[Δ] Beatrice Gorelli,[Δ] Simona Saponara,[Δ] Mascia Benedusi,[€] Alessandra Pecorelli,[‡] Patrizia Minetti,[∫,†] Giuseppe Valacchi,[‡,€,↕] Stefania Butini,[§,] Giuseppe Campiani[§,*] Sandra Gemma,[§,°] Mauro Maccarrone,[#,¶,°] Giuseppe Di Giovanni[£,◊,°]*

[§]Department of Excellence of Biotechnology, Chemistry and Pharmacy, 2018-2022, University of Siena, Via Aldo Moro 2, 53100, Siena, Italy; [¥]Department of Experimental Medicine Tor Vergata University of Rome, Via Montpellier 1, 00121 Rome, Italy; [£]Laboratory of Neurophysiology, Department of Physiology and Biochemistry, Faculty of Medicine and Surgery, University of Malta, Msida, Malta; [♪]Dept. of Experimental and Clinical Medicine, Section of Neuroscience and Cell Biology, Università Politecnica delle Marche, 60126 Ancona Italy; [¥]Department of Pharmacy, University of Pisa, Via Bonanno 6, 56126, Pisa, Italy; [¶]European Center for Brain Research/IRCCS Santa Lucia Foundation, Via del Fosso di Fiorano 64, 00143 Rome, Italy; [$]Pittsburgh Inst. for Neurodegenerative Dis. and Dept. of Neurology, Univ. of Pittsburgh, PA, USA; [Δ]Department of Life Sciences, University of Siena, Via Aldo Moro, 2, Siena , Italy; [€]Department of Biomedical and Specialist Surgical Sciences, Section of Medical Biochemistry, Molecular Biology and Genetics, University of Ferrara, Ferrara, Italy; [‡]Plants for Human Health Institute, Animal Science Dept., NC Research Campus, NC State University, 600 Laureate Way, Kannapolis, NC, 28081, USA; [∫]Sigma Tau, Via Pontina Km 30,400, 00040 Pomezia, Italy; [↕]Kyung Hee University, Department of Food and Nutrition, Seoul, South Korea; [#]Department of Biotechnological and Applied Clinical Sciences, University of L'Aquila, Via Vetoio snc, 67100 L'Aquila, Italy; [◊]Neuroscience Division, School of Biosciences, Cardiff University, Cardiff, UK.

Abstract

Temporal lobe epilepsy is the most common form of epilepsy and current antiepileptic drugs are ineffective in many patients. The endocannabinoid system has been associated with an on-demand protective response to seizures. Blocking endocannabinoids' catabolism would elicit antiepileptic effects, devoid of psychotropic effects. We herein report the discovery of selective anandamide catabolic enzyme fatty acid amide hydrolase (FAAH) inhibitors with promising antiepileptic efficacy, starting from a further investigation of our prototypical inhibitor **2a**. When tested in two rodent models of epilepsy, **2a** reduced the severity of the pilocarpine-induced status epilepticus and the elongation of the hippocampal maximal dentate activation. Notably, **2a** did not affect hippocampal dentate gyrus long-term synaptic plasticity. These data prompted our further endeavor aiming at discovering new antiepileptic agents, developing a new set of FAAH inhibitors (**3a-m**). Biological studies highlighted **3h** and **3m** as the best performing analogues to be further investigated. In cell-based studies, using a neuroblastoma cell line, **3h** and **3m** could reduce the oxinflammation state by decreasing DNA-binding activity of NF-kB p65, devoid of cytotoxic effect. Unwanted cardiac effects were excluded for **3h** (Langendorff perfused rat heart). Finally, the new analogue **3h** reduced the severity of the pilocarpine-induced status epilepticus as observed for **2a**.

Keywords: Endocannabinoid system; Fatty acid amide hydrolase; Enzyme inhibitors; Selective inhibitors; Epilepsy; Temporal lobe epilepsy; Seizures

Introduction

The endocannabinoid system (ECS) is a modulatory system orchestrated by endocannabinoids, their receptors, transporters, biosynthetic and catabolic enzymes. The most important endocannabinoids, namely arachidonoylethanolamide (or anandamide, AEA) and 2-arachidonoyl-glycerol (2-AG) are fatty acid-derived messengers endowed with major pro-homeostatic functions. They are synthesized "on-demand" from membrane phospholipids precursors and mainly exert their action by interacting with type 1 and type 2 cannabinoid receptors (CB1Rs and CB2Rs). Their activity is terminated after enzymatic degradation that is principally exerted by fatty acid amide hydrolase (FAAH, for AEA) and monoacylglycerol lipase (MAGL, for 2-AG).[1] The ECS regulates relevant signaling pathways including excitotoxicity, neurodegeneration, oxidative stress (OS) and neuroinflammation. Particularly, a reduction of AEA was ascertained in patients affected by temporal lobe epilepsy (TLE).[2] However, the neuroprotective role of AEA was confirmed by the kainic acid-induced increase of AEA in the hippocampus provides, without affecting 2-AG, "on-demand" protection against acute excitotoxicity. Seizure activity initiates cellular Ca^{2+} influx through NMDA and voltage-gated channels thus increasing the activity of pro-oxidant systems.[3] The EC system can delay or prevent excitotoxic damage (by re-balancing the excitatory/inhibitory systems) and OS-related epileptogenesis.[4] On these bases, a safe, promising, and viable method to attain a therapeutic effect would be the potentiation of the ECS tone by inhibition of the endocannabinoids' catabolic enzymes, such as the FAAH enzyme. This approach would elude the occurrence of unwanted psychotropic side effects that accompany the administration of CBR agonists.[5] As a further advantage, FAAH inhibition could provide higher selectivity as it would locally increase the activity of the ECS, at sites where endocannabinoids are produced.[6] For these reasons,

remarkable efforts have been made both by academia and pharmaceutical companies to develop potent and selective FAAH inhibitors.

Epilepsy is a neurological disorder clinically defined by the International League Against Epilepsy (ILAE).[7] In developed countries epilepsy has a prevalence ranging from 4-10 cases per 1000[8] and an incidence of 43.4 per 100,000 people per year.[9] Developing countries have a higher prevalence with a range of 14-57 cases per 1000[10] and also a higher incidence of 68.7 per 100,000 people per year.[9] Although there have been few epidemiological studies into TLE, they indicate that TLE accounts for around 60-70% of epilepsy cases[11-13] making it the most common type of focal epilepsy. Seizures have a myriad of acute effects such as loss of consciousness, tonic muscle contractions, colonic jerking and postictal confusion. There are also comorbidities such as depression and anxiety[14] and long-term effects of epilepsy including neuronal cell loss with associated memory deficits.[15] Mechanisms of brain damage and neuronal loss associated with epilepsy are multi-factorial including mitochondrial dysfunction, OS and inflammation (i.e. oxinflammation phenomenon[16, 17]) leading to seizure-mediated lipoperoxidation damage which may affect the cellular ionic balance.[18, 19]

Although cases of epilepsy commonly have a good prognosis, the disorder is associated with a higher mortality rate arising from causes such as accidental trauma, drowning, and suicide.[8] Though some effective antiepileptic drugs exist, a recent study estimated that about 140,000 patients exist in the USA with drug-resistant TLE[20] thus indicating the pressing need for new therapeutic options for this type of epilepsy.

In the last decades, ECS has become a focus of research in many conditions including epilepsy. The endocannabinoids play a key role in neuromodulation by retrograde signaling.[21] Activation of CB1R inhibits neurotransmitters' release; therefore, it may induce depolarization-

induced suppression of inhibition (DSI) or depolarization-induced suppression of excitation (DSE) depending on if the CB1Rs are on GABAergic or glutamatergic neurons, respectively.[22] Unsurprisingly, a neuromodulatory system of such widespread importance in the brain has been implicated in the etiopathogenesis of epilepsy and changes in the ECS were documented in animal models of epilepsy, as well as in humans. CB1Rs expression was found reduced in the thalamus of epileptic rats.[23] In human patients with untreated TLE there is a reduced amount of AEA in the cerebrospinal fluid.[2] Further, the increased CB1Rs expression on GABAergic neurons or the increased sprouting of CB1Rs expressing GABA axons[24] supports previous knowledge of the involvement of GABA in seizures.[25]

In this context, the involvement of the endocannabinoids in excitatory/inhibitory balance mechanisms in the brain, and their selective impairment in distinct neurological disorders, offers a glimpse for novel therapeutics.[26] In fact, as a result of the neuroprotection offered by the ECS, this latter has become a target for potential treatment in various neurological disorders, such as Huntington's disease,[27] Alzheimer's disease[28] and epilepsy.[5] The stimulation of ECS may exert neuroprotective effects and a rapid increase in AEA levels during seizures in mice providing a CB1R mediated protection against excitotoxicity.[29] Accordingly, some CB1R agonists (e.g. Δ9-THC and WIN-55,212)[30] proved to be antiepileptic. However, their administration can alter synaptic plasticity with inhibition of long-term potentiation[31] likely the cause of impairment in cognition and the detrimental effects on long-term memory.[32, 33] Prolonged use of WIN-55,212 can also lead to a reduction in its antiepileptic efficacy due to tolerance and alterations in CB1Rs expression.[34]

In the context of indirect agonism of the ECS, FAAH inhibitors such as URB-597 (**1**, Figure 1)[35] and hexadecyl sulfonylfluoride, namely AM374[36] have previously shown promising

antiepileptic and neuroprotective activities. Other FAAH inhibitors showed differing effects on memory, which in many cases have a better profile than CB1R agonists,[37] as also recently demonstrated by our team in TLE.[38]

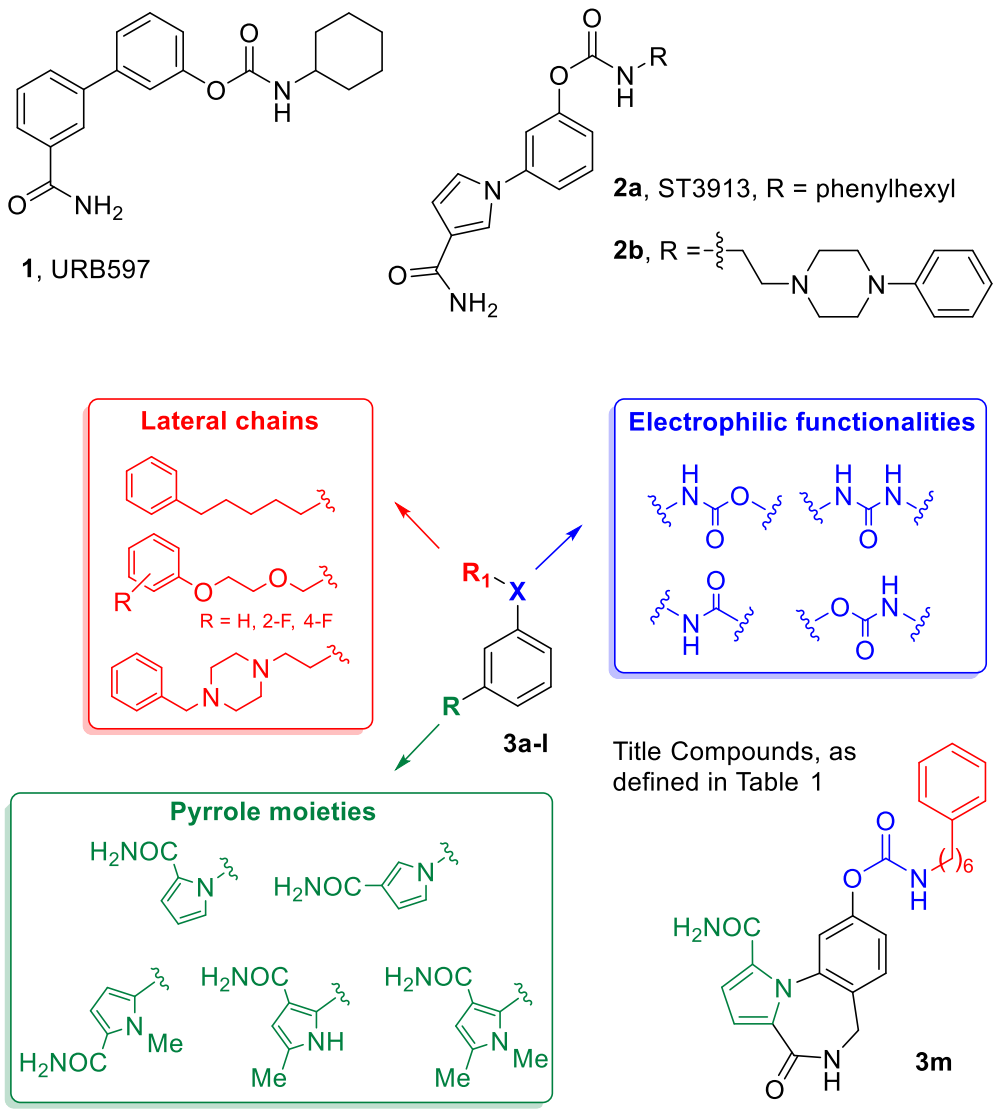

Figure 1. Reference compounds (**1–2a,b**) and title compounds (**3a–m**).

Recently,[39-42] we identified a potent and selective FAAH inhibitor hit, namely ST3913 (**2a**, Figure 1). Since the efficacy of **2a** was never measured before in animal models of epilepsy, this manuscript deals with the *in vivo* characterization of the antiepileptic potential of **2a** in two rodent models of epilepsy, the identification of a new class of FAAH inhibitors (**3a-m**, Figure 1)

along with their biological investigation leading to the selection of **3h** to be tested *in vivo* to measure its antiepileptic potential.

In particular, after i.p. administration, **2a** proved to be efficacious in the pilocarpine and the maximal dentate activation murine models of TLE during seizures and using it as a pretreatment. In addition, we have investigated the effect on synaptic plasticity (short-term and long-term plasticity STP-LTP) and neuronal damage resulting from seizures (the histological study of thiols formations).

The encouraging data obtained with **2a** have prompted us to further expand the series of phenylpyrrole-based analogues in the quest of identifying further potent and selective FAAH inhibitors as new antiepileptic agents to be used as a follow-up of **2a**. Accordingly, we initiated a further medicinal chemistry endeavor developing a new set of FAAH inhibitors (**3a-m**, Figure 1). We herein report the synthesis, molecular modelling and biological investigation of this new set of molecules (**3a-m**) structurally related to **2a**. Computational methods were used for a preliminary evaluation of the drug-like profile and of the physicochemical properties of the developed compounds and for a rational analysis of the structure-activity relationships (SAR). The most interesting inhibitors of the new series, **3g**, **3m** and **3h**, were selected for further studies. Selectivity towards CB1R, CB2R and MAGL was assessed for the new analogues. For compound **3h** preliminary metabolic stability studies were performed, by incubation with human and rat liver microsomes. Cytotoxicity of compounds **3g** and **3h** was measured on mouse fibroblasts, and the absence of mutagenicity was observed by Ames test. Notably, compounds **3h** and **3m** demonstrated a potential anti-oxinflammatory profile on the neuroblastoma cell line (IMR32), by decreasing the LPS-induced activation of the redox-sensitive transcription factor NF-κB p65. The absence of cardiac toxicity was determined for compound **3h** in Langendorff

isolated heart model. These data allowed the selection of the newly identified FAAH inhibitor **3h** for *in vivo* studies. Gratifyingly, the newly developed analogue **3h** has replicated the antiepileptic potential of **2a** in the pilocarpine model, confirming the notable potential for this class of analogues against seizures.

Results and Discussion

Chemistry

The synthesis of compounds **3a-m** is reported in Schemes 1-3. As described in Scheme 1 the 1-(3-aminophenyl)-1*H*-pyrrole-3-carbonitile (**4**)[43] was identified as the key intermediate for the synthesis of the "inverted" carbamates (**3a-d**, Table 1) and the urea (**3e**, Table 1). Derivative **4** was easily converted, using phosgene, in the intermediate isocyanate that reacted with 6-phenylhexan-1-ol (**5a**), or with the differently functionalized phenoxyethoxyethyl alcohols (**5b-d**),[39] to afford the corresponding carbamates (**6a-d**). From compounds **6a-d**, after partial hydrolysis of the cyano group performed with perborate, compounds **3a-d** were obtained. The hydrolysis of the cyano group of **4**, in the presence of hydrogen peroxide and sodium hydroxide, allowed the isolation of 1-(3-aminophenyl)-1*H*-pirrole-3-carboxamide (**7**[43]). Compound **7** was identified as the substrate for a convergent approach in which it was reacted with 6-phenylhexan-1-yl-isocyanate[39] leading to the urea derivative **3e**. The amidic derivative **3f** was obtained from the acid **8**, after treatment with triphenylphosphine and hexachloroacetone, in presence of 6-phenylhexan-1-amine followed by basic hydrolysis of the cyano portion of the intermediate **9**. Acid **8** could be synthesized as previously described by a Clauson-Kaas reaction,[40] but we herein report a slight elaboration of the originally employed[44] reaction protocol that has allowed a substantial improvement of the reaction yield (see Experimental Section for details).

Scheme 1. Synthesis of the "inverted" carbamates **3a-d**, ureas **3e**, and amide **3f**.

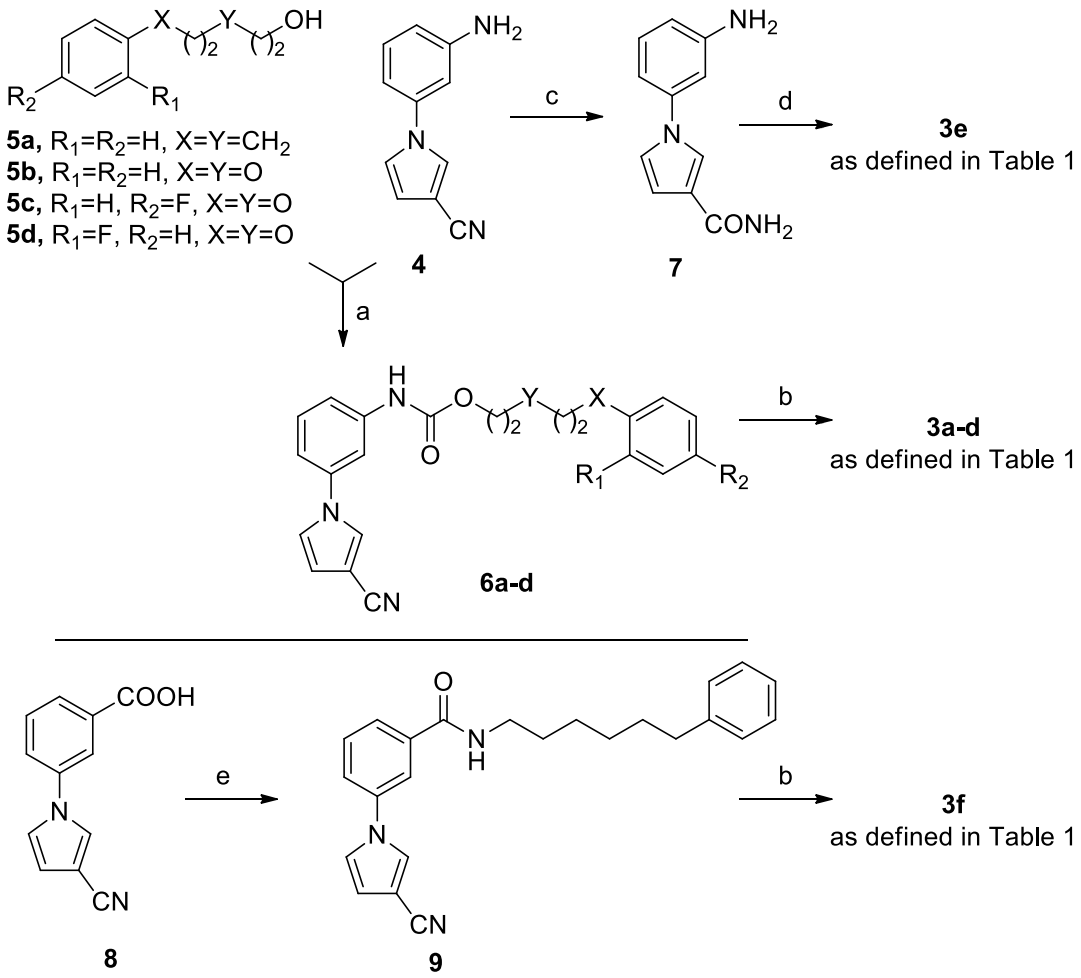

Scheme 1. Reagents and conditions. a) $COCl_2$ (20% solution in toluene), pyridine, dry DCM, 25 °C, 12 h, then appropriate alcohol, TEA, dry THF, reflux, 12 h, 14-69%; b) $NaBO_3$ x $4H_2O$, 1,4-dioxane, H_2O, 80 °C, 1,5 h. 25-40%; c) 6 M NaOH, 30% H_2O_2, EtOH, reflux, 12 h, 90%; d) 6-phenylhexan-1-yl-isocyanate, TEA, dry THF, reflux, 12 h, 40-62%; e) PPh_3, $(Cl_3C)_2CO$, 6-phenylhexan-1-amine, dry DCM, TEA, from 0 °C to 25 °C, 1 h, 30%.

Scheme 2. Synthesis of the carbamates **3g-l**.

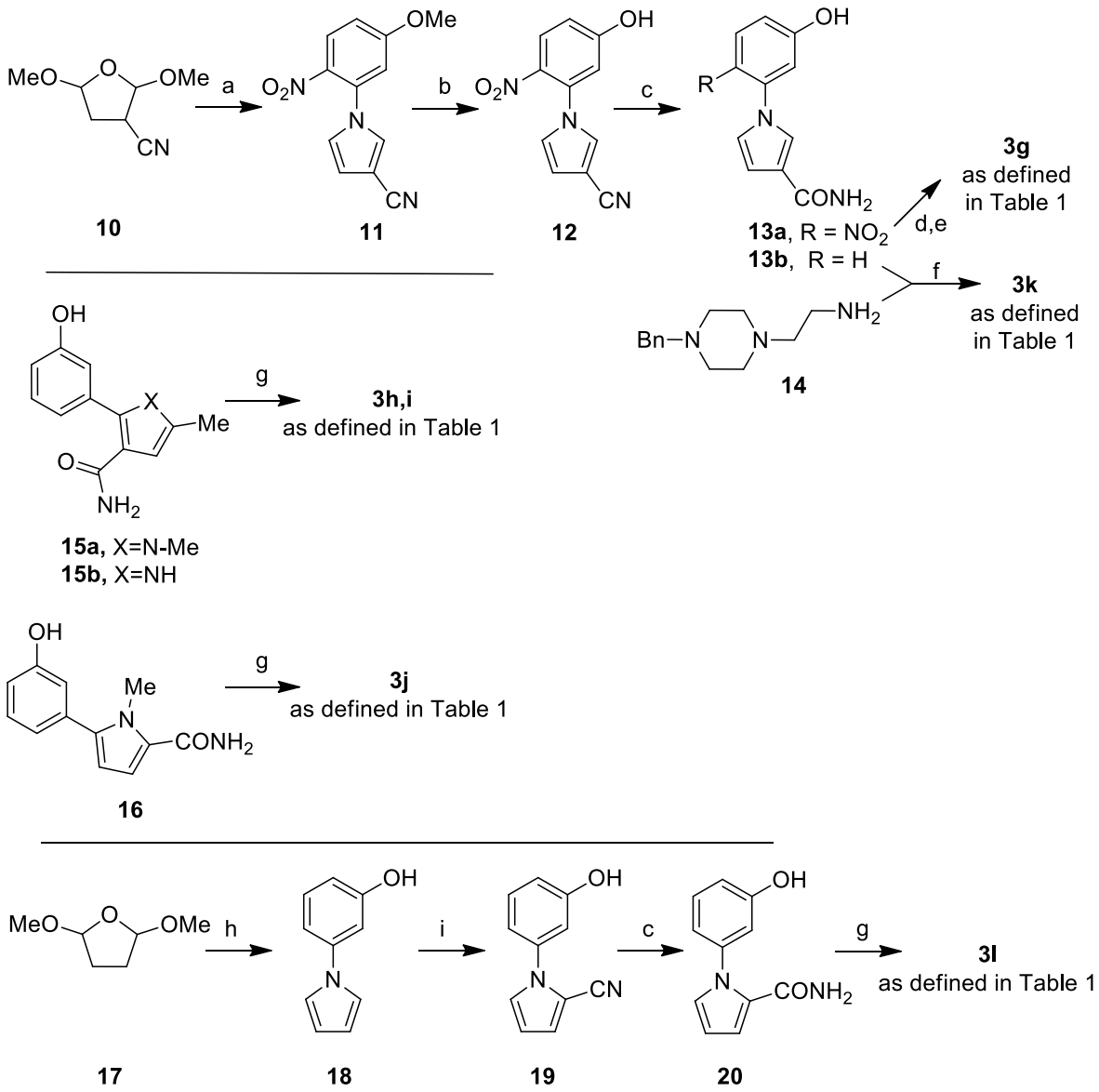

Scheme 2. Reagents and conditions. a) 5-Methoxy-2-nitroaniline, 6M HCl, 1,4-dioxane, reflux, 40 min. 87%; b) BBr_3, dry DCM, from -78 to 25 °C, 12 h, 50%; c) 6M NaOH, 30% H_2O_2, EtOH, reflux, 12 h, 50%; d) 6-phenylhexan-1-yl-isocyanate, TEA, dry toluene/DMF, (4:1), reflux, 48 h e) H_2, 10% Pd/C, 15 psi, EtOH, 25 °C, 3 h, 45% (over 2 steps); f) DMAP, $COCl_2$ (20% solution in toluene), THF dry, from 0 to 70 °C, 16 h, 20%; g) 6-phenylhexan-1-yl-isocyanate, TEA, dry THF, reflux, 12 h, 20-79%; h) 3-aminophenol, AcOH, MW, 170 °C, 10 min. 80%; i) $ClSO_2NCO$, dry MeCN, from -20 to 25 °C, 12 h; then dry DMF, 55 °C, 30 min, 20%.

2,5-Dimethoxytetrahydrofuran-3-carbonitrile (**10**) (Scheme 2) was subjected to a Clauson-Kaas reaction with 5-methoxy-2-nitroaniline to afford the key phenyl-pyrrole intermediate (**11**). After cleavage of the anisolic portion (**12**) and partial hydrolysis of the nitrile functionality, the carboxamide **13a** was achieved. Finally, the treatment of **13a** with 6-phenylhexan-1-yl-

isocyanate, followed by reduction of the nitro group by catalytic hydrogenation, afforded the compound **3g**.

For the synthesis of **3k**, a convergent approach exploited phenylpyrrole-3-carboxamide **13b**[39] which, after transformation into the correspondent chloroformate, by using phosgene, was reacted with the 2-(4-benzylpiperazin-1-yl)ethan-1-amine (**14**) that was prepared as reported.[45] Derivatives **15a,b**, and **16** were synthesized as described[42] and, by reaction with 6-phenylhexan-1-yl-isocyanate, transformed into the correspondent urethanes **3h-j**. The Clauson-Kaas reaction between 3-aminophenol and 2,5-dimethoxytetrahydrofuran **17** was performed in the presence of acetic acid under microwave irradiation allowing a fast, clean and high yielding option to obtain the 1-(3-hydroxyphenyl)pyrrole **18** that substantially improved the previously reported yields.[46, 47] This latter was subjected to a cyanation reaction using chlorosulfonyl isocyanate in the presence of DMF, affording the cyanoderivative **19**. After hydrolysis of **19**, the corresponding amide **20**, was reacted with 6-phenylhexan-1-yl-isocyanate in order to obtain compound **3l**.

The intermediate **21**[41] (Scheme 3) was subjected to a bromination reaction affording a mixture of isomers of mono- and di-brominated compounds. After column chromatography, we could isolate pure isomer **22** as a major product, which was crystallized from EtOAc and subjected to X-ray diffraction analysis to clarify the exact structure. This analysis unambiguously indicated the bromine at C alpha position of the pyrrole system (C1 of Figure 2). Our efforts to characterize the other isomers were hampered by the low amount obtained and by its contamination by the inseparable di-brominated product. Compound **22** was then converted into its cyano-derivative counterpart **23**, which after demethylation afforded the phenol **24**. Nitrile hydrolysis (**25**) and reaction with 6-phenylhexan-1-yl-isocyanate, allowed the isolation of the tricyclic analogue **3m**.

Scheme 3. Synthesis of the tricyclic analogue **3m**.

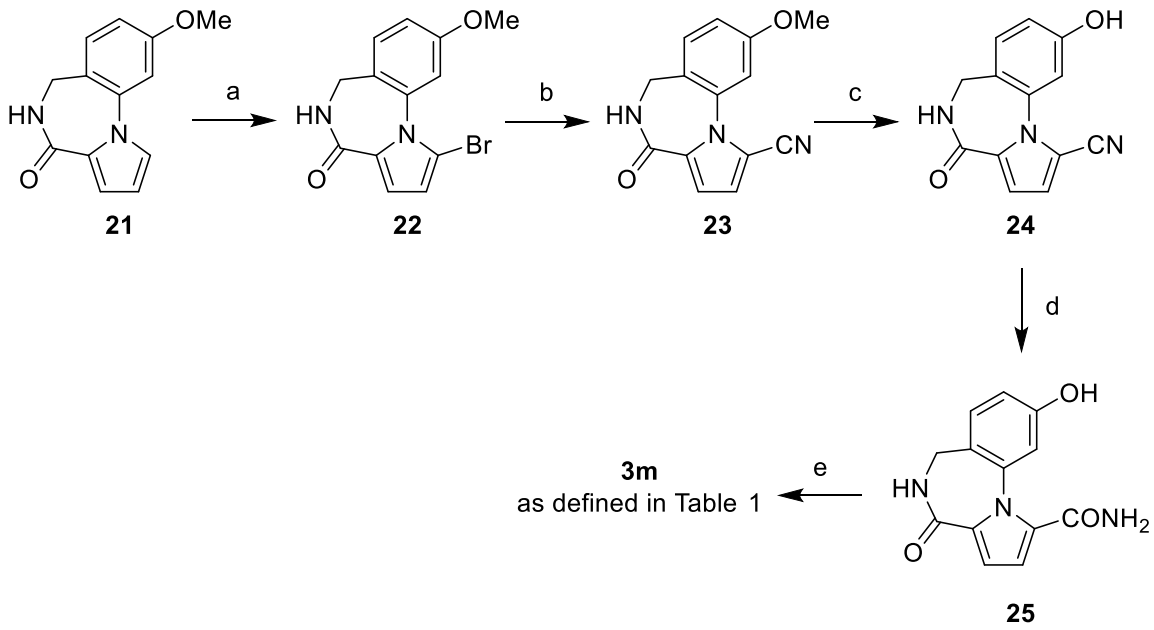

Scheme 3. Reagents and conditions. a) NBS, dry THF, -78 °C to 25 °C, 12 h, 45%; b) CuCN, dry DMF, reflux, 12 h, 30%; c) BBr_3, dry DCM, from -78 to 25 °C , 12 h, 30%; d) 6M NaOH, 30% H_2O_2, EtOH, reflux, 12 h, 40%; e) 6-phenylhexan-1-yl-isocyanate, TEA, dry THF, reflux, 12 h, 50%.

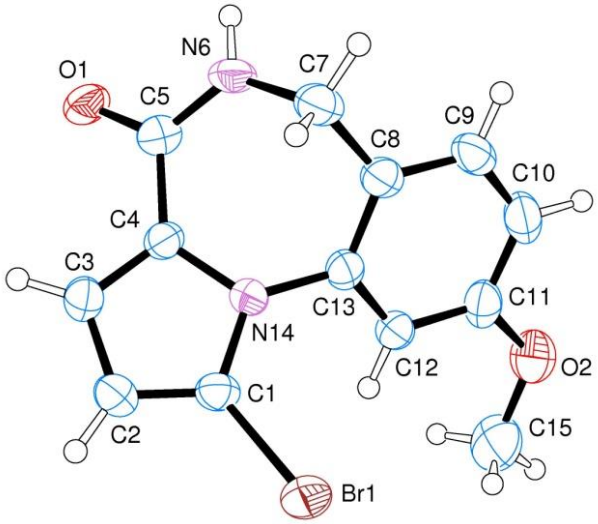

Figure 2. Crystal structure of the bromo-substituted compound **22**. Ellipsoids enclose 50% probability.

Table 1. Inhibition activity towards mouse brain FAAH (as IC_{50} nM) for compounds **3a−m** and reference compounds **1**, and **2a,b**.

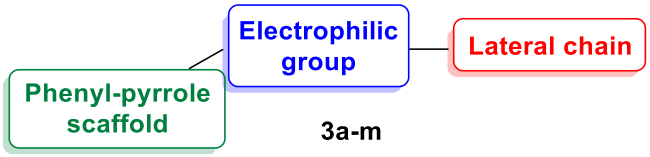

Cmpd	Phenyl-pyrrole scaffold	Elect. Group	Lateral Chain	IC_{50} (nM)[a] or inhibition %[b]
3a	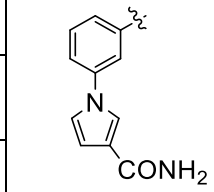	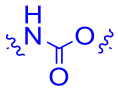	phenylhexyl	30000 ± 6000 (13000-69000)
3b			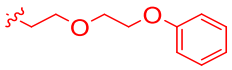	19% @100 μM
3c			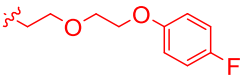	53% @100 μM
3d			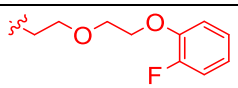	56% @100 μM
3e		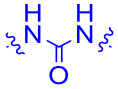	phenylhexyl	7500 ± 1200 (3800-15000)
3f			phenylhexyl	37% @100 μM
3g	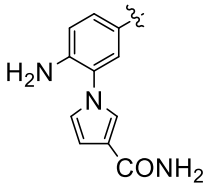	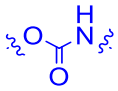	phenylhexyl	1.10 ± 0.10 (0.73-1.60)
3h	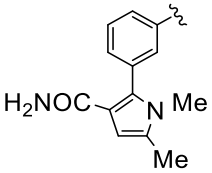		phenylhexyl	6.88 ± 0.38 (4.50-11.37)
3i	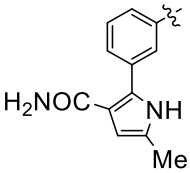		phenylhexyl	42.0 ± 6.5 (13.5-133.0)
3j	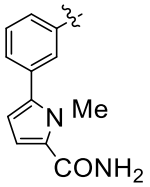	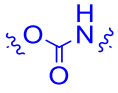	phenylhexyl	9.1 ± 3.5 (1.8-25.0)

3k	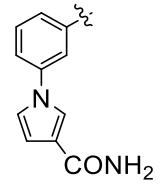	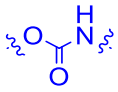	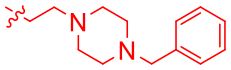	24% @100 nM
3l	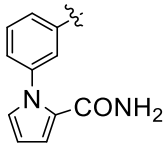	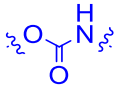	phenylhexyl	59 ± 13 (39-86)
3m	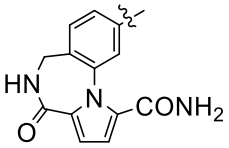	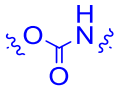	phenylhexyl	35 ± 8 (16-75)
1 URB597	-	-	-	11.5 ± 2.3
2a[39] ST3913	-	-	-	0.60
2b[42]	-	-	-	58

[a]Each value is the mean of at least two experiments (95% confidence intervals are into brackets).

Structure-activity relationship and molecular modelling studies

As a continuation of our endeavours in the discovery of potent FAAH inhibitors, we have developed a new series of pyrrole-based analogues (**3a-m**, Figure 1 and Table 1). In this new series of compounds our structural hit **2a** was modified, at i) the electrophilic centre ii) the lateral chain and iii) the pyrrole moiety. These modifications were used to investigate the SARs and to implement the pharmacokinetic properties such as the metabolic stability (by fluorination and the use of different pyrrole systems) and the solubility profile (lateral chains and scaffold modifications) of the developed compounds over the parent **2a**. In particular, the original carbamate moiety of **2a** was "inverted" as in compounds **3a-d**, a urea moiety was introduced in derivative **3e**, and in compound **3f** we evaluated the effect of an amide system. As regards the lateral chains, we explored the replacement of the hexamethylene spacer of **2a** by a poly-ethereal chain (**3b-d**) or piperazine containing chain (**3k**). Further, in the phenyl system of the lateral

chain, some fluorine atoms were introduced (compounds **3c,d**) to improve metabolic stability. As regards the central core of the molecules, in **3g** we introduced an amino group (aniline) in the phenyl system and we varied the junctions with differently decorated pyrrole systems (**3h-j,l**). Following the results of our previous studies[41] a rigidification by bridging the phenyl-pyrrole scaffold of **3l** was applied leading to the tricyclic analogue **3m**.

The FAAH inhibition potencies of the newly developed compounds (**3a−m**) were assessed using enzymatic studies performed on the mouse brain FAAH and allowed us to decipher the SARs useful for the selection of the best compounds of the series. Our studies indicated that the potency of the compounds is affected by the nature of the electrophilic groups, as all the evaluated modifications (**3a-f**) led to less potent compounds when compared to **2a**. Amongst the modifications introduced on the lateral chains, our studies revealed that the introduction of fluorine atoms, or phenoxy-ethoxyethyl groups (as in the sub-series of compounds **3b-d**) was detrimental for activity. In fact, compounds **3b-d** caused only 19-56% inhibition of FAAH when tested at 100 μM (Table 1). As compared to these analogues, the piperazine containing chain was better tolerated when installed on a carbamoyl-based analogue and compound **3k** showed 24% FAAH inhibition when incubated at 100 nM (Table 1). In fact, the most potent inhibitors belong to the sub-series of phenol-carbamate-based analogues with a phenylhexyl lateral chain (**3g-j,l,m**, Table 1). As expected, compound **3g** exhibited a potency of inhibition in the nanomolar range (**3g**, IC_{50} = 1.10 nM, Table 1) comparable to that of our lead **2a** while compound **3l** displayed an encouraging two-digit nanomolar potency for enzyme inhibition, demonstrating that the positioning of the amide at C-2 of the pyrrole system could be well tolerated by the enzyme. This evidence prompted us to synthesize the rigidified tricyclic analogue **3m**, which nicely challenged the activity of **3l**. As per our initial interest, we sought to understand the SARs

derived by changing the pyrrole junctions. Accordingly, we synthesized compounds **3h-j**. The 2-phenyl-1,5-dimethyl-1*H*-pyrrole-3-carboxamide core, embedded in compound **3h**, resulted in the best performing system when compared to the 2-phenyl-5-methyl-1*H*-pyrrole-3-carboxamide of **3i** or the 5-phenyl-1-methyl-1*H*-pyrrole-2-carboxamide of **3j**. Though all the three analogues behave as potent FAAH inhibitors (Table 1) compound **3h** (IC_{50} = 6.88 nM) resulted in the most potent inhibitor of this sub-series of analogues and was further assayed in biological tests.

To gain information about the possible binding modes of the tested compounds into the humanized variant of rat FAAH protein (*h*/*r*FAAH) binding site, we performed molecular docking calculations employing the Induced Fit Docking (IFD) technique.[41, 43] Starting with **3a** bearing an "inverted" carbamate moiety (Figure S1A), we observed a weak interaction within the binding site of the enzyme and details are provided in the Supplementary Information (SI) file. These data appear to be in line with the micromolar inhibitory potency of the compound. In compounds **3b-d** the introduction of a polyether tether resulted in a dramatic decrease of the inhibitory activity. Accordingly, for these compounds (**3b-d**, Figure S1B-D) we detected weak contacts with the active site of the enzyme (see SI for details). The transformation of the electrophilic functionality from the "inverted" carbamate to urea led to **3e** that, with inhibition potency below 10 μM, improved the efficacy over **3a**, as also outlined by our computational studies (Figure S1E, and SI). In compound **3f** the change of the electrophilic functionality into an amide did not produce any improvement in potency with respect to the previously discussed compounds. However, the presence of an amide in place of the urea group made **3f** able of establishing an H-bond with Q273 (Figure S1F, and SI for details).

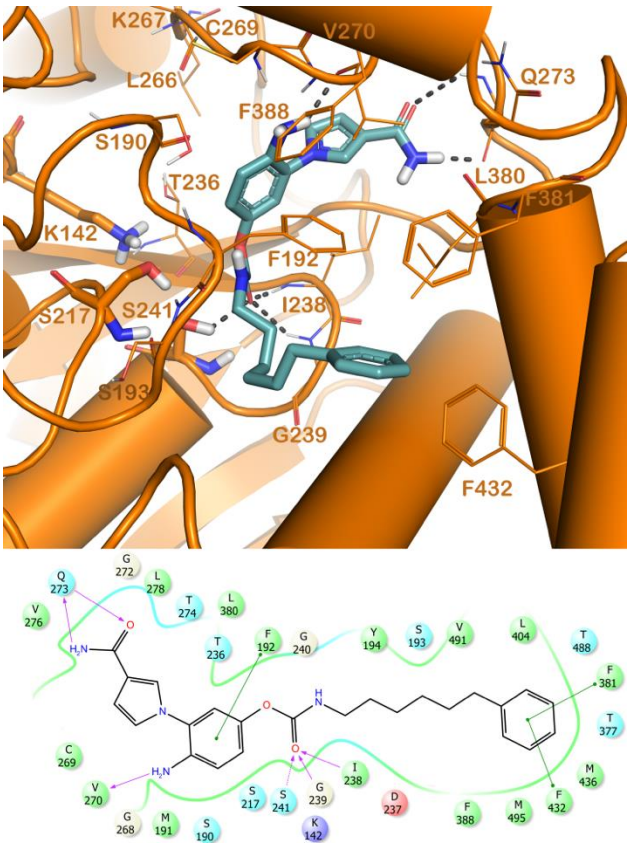

Figure 3. Binding mode of **3g** (light blue sticks) into *h/r*FAAH enzyme (orange cartoon, PDB ID: 3PPM) binding site. The residues forming the catalytic triad (K142, S217 and S241) are reported in sticks while the other residues of the binding site are reported as lines. The non-polar hydrogens were removed for clarity. The picture was generated by means of PyMOL.

A carbamate group, as the electrophilic functionality, and a NH_2 in the benzylpyrrole moiety characterize the compound **3g**. As reported in Figure 3, **3g** made strong interactions with the active site of the enzyme. This compound, despite the presence of an NH_2 moiety at *para*-position with respect to the electrophilic group, still maintains a good FAAH inhibition potency, as already observed for other FAAH inhibitors.[48] The carboxamide moiety formed two H-bonds with the backbone of Q273, the central region targeted F192 by a π-π stacking, while the NH_2 substituent H-bound V270. The carbamate moiety strongly interacted in the catalytic region of

the enzyme with the catalytic S241 and with I238 and G239 (oxyanion hole) by a network of H-bonds. The phenylhexyl chain established a double π-π stacking with F381 and F432. Remarkably, the orientation of the carbon of the carbamate portion and its distance from the catalytic residue S241 (< 3 Å) could be in agreement with a potential nucleophilic attack. In general, the strong pattern of interaction within the binding site accounts for an inhibitory activity in the low nanomolar range (Table 1), making **3g** one of the best performing compounds of the series.

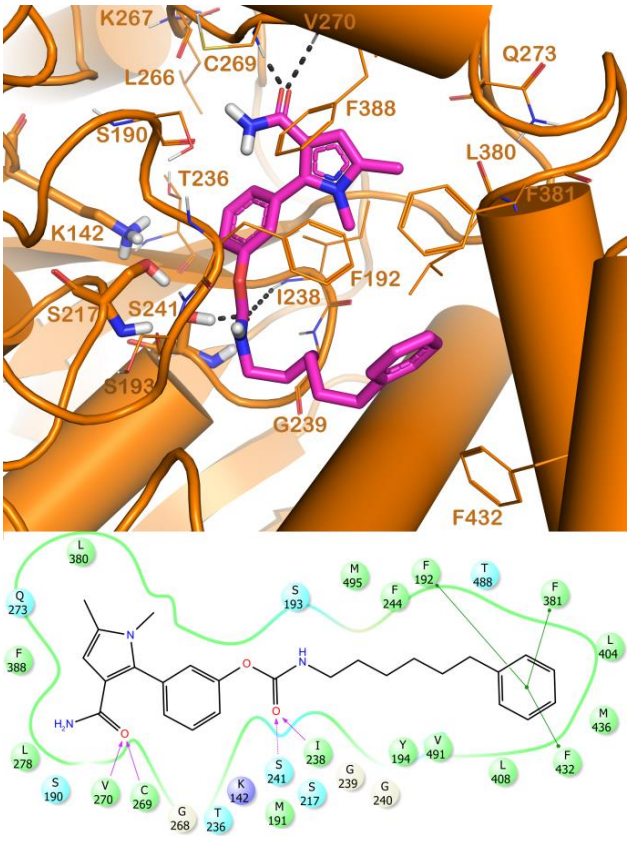

Figure 4. Binding mode of **3h** (magenta sticks) into *h/r*FAAH enzyme (orange cartoon, PDB ID: 3PPM) binding site. The residues forming the catalytic triad (K142, S217 and S241) are reported in sticks while the other residues of the binding site are reported as lines. The non-polar hydrogens were removed for clarity. The picture was generated by means of PyMOL.

The nanomolar FAAH inhibitors **3h-j**, bear differently decorated pyrrole systems (Figure 4 and Figures S2A,B). For **3h** we registered one of the best inhibitory profiles of the series (Table 1). In particular, **3h** H-bound the backbone of C269 and V270 by its carboxamide moiety (Figure 4). The carbamate moiety H-bound S241 and I238 (oxyanion hole). As for **3g**, the distance between the carbon of the carbamate and the catalytic S241 could be in agreement with a potential nucleophilic attack. The phenylhexyl chain established a triple π-π stacking (F192, F381 and F432). Compound **3i** differs from **3h** for the absence of methyl in the nitrogen of the pyrrole ring. This difference allowed maintaining the same contacts described for **3h,** with exception of a H-bond with the oxyanion hole (see SI and Figure S2A) that may explain the reduction of the inhibitory potency as compared to **3h**. The shifting of the amide system to position 5 of the pyrrole system led to the analogue **3j** that, besides interaction with S241 and I238, also interacted with S193 (see SI Figure S2B).

The introduction of a benzylpiperazine in the nucleus of **2a**, led to compound **3k**. Few contacts were found with the FAAH enzyme leading to a decreased affinity (see SI and in Figure S2C).

The presence of the phenylhexyl lateral chain, combined with a phenyl-1-pyrrole scaffold substituted by a carboxamide group at C2 of the pyrrole ring as in **3l**, allowed strong interactions with the key residues of the enzyme. In fact, the carboxamide group of **3l** formed H-bonds with C269 and V270 that, with the other classical contacts (SI and Figure S2D), accounted for an inhibitory profile in the nanomolar range. Finally, a rigidification by bridging the phenylpyrrole scaffold of **3l** led to the tricyclic analogue **3m**. The docking output (Figure 5) showed the same interactions found for **3l** with the exclusion of the H-bond with S193. However, compound **3m** can target the backbone of T236, by its carboxamide group forming an H-bond, and residue F192, by its phenylpyrrole moiety establishing a π-π stacking. The phenylhexyl lateral chain π-π

stacks with F381 and F432. This slight improvement in terms of the number of contacts accounted for a slight increase in the binding affinity with respect to its parent compound **3l**.

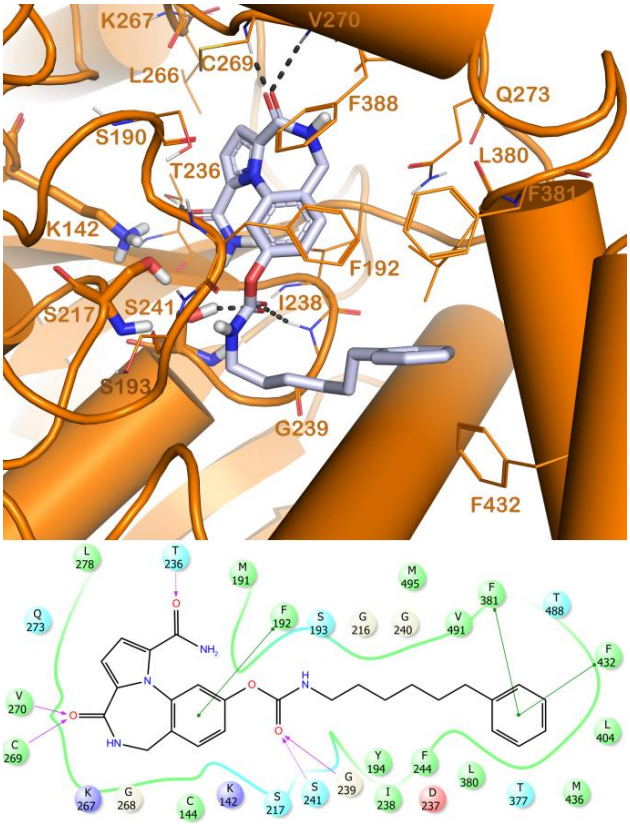

Figure 5. Binding modes of **3m** (light gray sticks) into *h/r*FAAH enzyme (orange cartoon, PDB ID: 3PPM) binding site. The residues forming the catalytic triad (K142, S217 and S241) are reported as sticks while the other residues of the binding site are reported as lines. The non-polar hydrogens were removed for clarity. The picture was generated by means of PyMOL.

For all the new compounds (**3a−m**) we also calculated the physicochemical properties using QikProp application. The output of this calculation is reported in the Supplementary Information (Table S1) along with a brief discussion. In particular, for compound **3h** we noted that, despite a low water solubility, the calculated oral absorption was amongst the best values of the series. For **3h** we could also predict the highest value of Caco2 permeability. Taken together with the

affinity and the toxicity data, **3h** exhibited favorable properties to be progressed for the *in vivo* studies.

Selectivity towards cannabinoid receptors and MAGL

We next interrogated the selectivity profile of the analogues **3h** and **3g** towards the murine receptors *m*CB1R and *m*CB2R (that possess an overall identity of 97.0% and 79.7 % with the *human* isoforms, respectively). Selectivity for the other relevant catabolic enzyme of the ECS (MAGL) was also measured. As depicted in Figure 6 none of the compounds showed issues of cross-reactivity with the tested proteins.

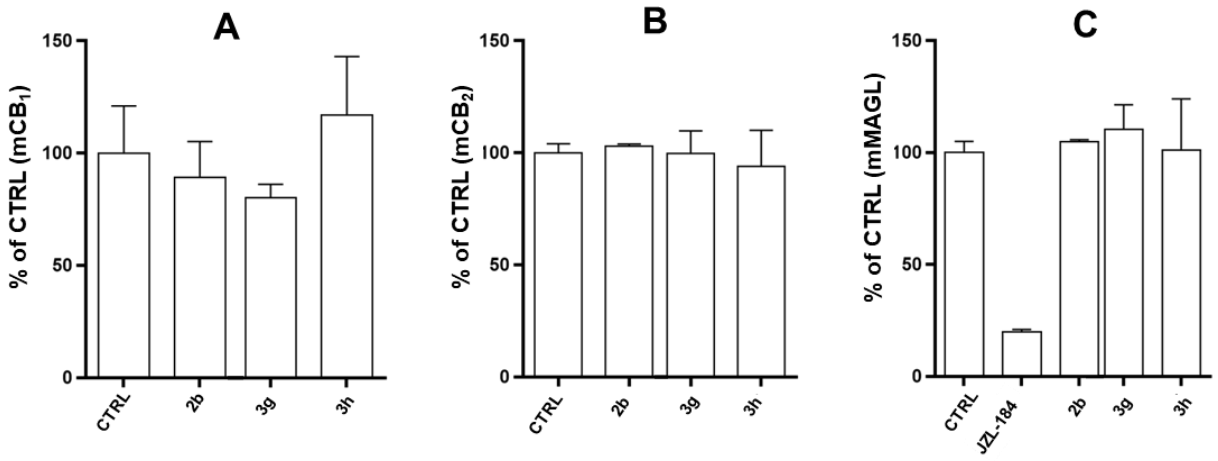

Figure 6. Selectivity of compounds **3h** and **3g** towards *m*CB1R (Panel A), *m*CB2R (Panel B), and *m*MAGL (Panel C), data for **2b** and the potent MAGL inhibitor JZL-184 are reported for comparison.

Cytotoxicity and mutagenicity profile evaluation for 3h and 3g

The potential cytotoxic profile was assessed for compounds **3h** and **3g** after incubation with mouse embryonic fibroblasts (NIH3T3 cell line), and with human glioblastoma astrocytoma cells (U373MG cell line).

The results, expressed as IC_{50} (μM), are reported in Table 2 and are compared with those obtained for the reference compounds **2a,b**. Gratifyingly, when tested on the NIH3T3 cells compound **3h** displayed low toxicity comparable to that of the hit analogues **2a** and **2b**. Also on the glioblastoma U373MG cell line **3h** exhibited a 46 μM IC_{50} value, very similar to that expressed by **2a**.

Table 2. Viability of mouse fibroblasts NIH3T3 and human glioblastoma astrocytoma cells U373-MG after incubation with **3h**, **3g** and reference compounds (as IC_{50} μM).

Cmpds	NIH3T3[a] IC_{50} (μM)	U373MG[a] IC_{50} (μM)
3h	69	46
3g	20	NT[b]
2a	75	50
2b	5	NT[b]

[a]Cell viability was measured by the Neutral Red Uptake (NRU) test and data normalized as % control; data are expressed as mean ± SD of 3 experiments repeated in 6 replicates; values are statistically different *vs* control, $p \leq 0.05$; [b]NT = not tested.

As further profiling, we used the Ames test as a reliable and widely used preliminary assessment for identifying potential risks of mutagenicity at the early stages of drug development. We ascertained for **3g** and **3h** the absence of mutagenic effect in the *Salmonella typhimurium* strains TA98 and TA100 (Figure S3). When performed in the presence of the S9 fraction of rat liver, the assay may serve also for assessing the potential mutagenicity risks derived from the compound's metabolites. By using these conditions, a more in-depth analysis of compound **3h** allowed us to exclude risks of toxicity also in the presence of the S9 fraction in both TA98 and TA100 *Salmonella typhimurium* strains (Figure S3).

Preliminary metabolic studies

The metabolic stability of **3h** and **2a** was assessed in human and rat liver microsomal preparations. The plot of non-metabolized compounds (%) versus time showed a monoexponential decay relationship (Figure 7).

For compound **3h** the apparent decay constants k were 0.0328 min^{-1} and 0.0704 min^{-1} for human liver microsomes (HLM) and rat liver microsomes (RLM), respectively. The resulted half-life time and Cl_{int} were, respectively, $t_{½}$ =21.4 and 10.5 min and Cl_{int} = 54.8 and 119.7 µL/min. The reference compound **2a** showed a lower intrinsic clearance in both microsomal preparations and presented lower microsomal stability in humans than in rat microsomal preparations. In fact, the calculated Cl_{int} were 55.5 and 39.2 µL/min in HLM and RLM, respectively.

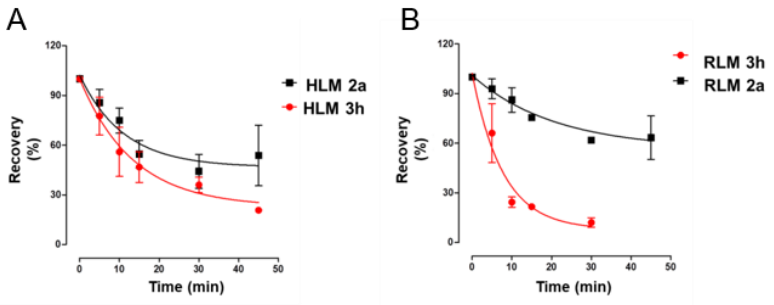

Figure 7. CYP-dependent metabolic depletion of 5 µM **3h** and **2a** in human (HLM, panel A) and rat liver (RLM, panel B) microsomal preparations. Results are presented graphically as percentage of compound recovery (100% at time 0 min) as a function of incubation time. Data are presented as mean ± SEM, of three different experiments.

When comparing the CYP-dependent metabolic depletion of compound **3h** compared to that of **2a** in RLM, we observed a higher metabolic liability of **3h**. On the contrary, in the HLM we

observed comparable profiles, even though with a slightly higher susceptibility to metabolism for **3h**.

These observations are relevant, though not being an issue hampering the *in vivo* efficacy of irreversible enzyme inhibitors. In fact, irreversible protein-inhibitors, being endowed with a longer duration of action as compared to reversible protein ligands, are less likely to suffer from poor pharmacokinetic parameters such as metabolic stability.[49] In fact, an irreversible ligand could require less frequent dosing being characterized by longer residence times and providing a higher degree of inactivation of the target protein. In line with these considerations, when we interrogated the effect of **3h** (see below in the *in vivo* studies section) in a rodent model of epilepsy, we observed an efficacy that paralleled that of **2a**.

Effect of 3h on Langendorff perfused rat heart

A major hurdle in the development of new drugs is reducing the risk of cardiac arrhythmias, such as long QT syndrome. To evaluate, and possibly exclude, the cardiotoxic potential of compound **3h**, its effect on cardiac mechanical function and electrocardiogram (ECG) in Langendorff-isolated rat hearts was assessed following our previously described protocol.[50]

Under control conditions, left ventricle pressure (LVP) and coronary perfusion pressure (CPP) values of 63 ± 2 and 51 ± 3 mmHg (n = 5), respectively, were obtained. At the maximum concentration tested (10 μM), **3h** increased LVP to 74 ± 2 mmHg (n = 5, ** $p < 0.01$, repeated measures ANOVA and Dunnett's post-test) and RR interval, while reducing HR. However, QTc values did not vary over the drug range tested (Table 3).

Table 3. Effects of **3h** on HR, RR, PQ, QRS, QT, and QTc in Langendorff Perfused Rat Hearts.

(μM)	HR (BPM)	RR (ms)	PQ (ms)	QRS (ms)	QT (ms)	QTc (ms)

none	259±6	232±5	37±1	14±0.5	76±4	76 ±4
0. 01	259±8	233±7	37±2	14±1	77±5	77±4
0.1	259±9	233±8	37±2	14±1	78±5	78 ±4
1	252±8	239±8	37±1	14±0.5	79±5	77 ±4
10	241±7**	250±8**	39±2	14 ±1	78±4	76±3

Each value represents mean ± SEM (n = 5 hearts). ** $p < 0.01$, repeated measures ANOVA and Dunnett's post test.

In summary, the collected data did not highlight a cardiotoxicity predictive of potential risk for a torsade de pointes for compounds **3h** at none of the concentrations tested which were three orders of magnitude higher than that effective in FAAH inhibition. **3h**, at the maximum concentration tested, behaved like a negative chronotropic and a positive inotropic agent on rat heart preparations.

Cytotoxicity determination and anti-oxinflammatory potential evaluation for 3h and 3m

Oxinflammation, a condition generated by harmful crosstalk between redox imbalance and inflammatory cascade, is a relevant issue in brain diseases and, in particular, in epilepsy.[17, 19] To explore the potential anti-oxinflammatory properties of two structural templates such as **3h** and the tricyclic analogue **3m**, first an evaluation of their cytotoxicity profile in IMR32 cell line was performed using the lactate dehydrogenase (LDH)-release assay. Different concentrations ranging from 0.1 μM to 50 μM of the compounds **3h**, **3m** and reference compound **2a** were tested and LDH release was determined after 24 h of treatment. As shown in Figure 8, no significant release of LDH into cell culture media was observed for all three compounds, demonstrating the lack of cellular toxicity at the concentrations analyzed. Based on these results, in the next experiment, IMR32 cells were first pre-treated with the compounds at the doses of 0.5 μM and 1 μM for 24 h and, then, challenged with 100 μg/mL LPS for 30 min. The ability of the

compounds **3h**, **3m** and **2a** to prevent the LPS-induced oxinflammatory signaling pathway was assessed by detecting specific NF-kB p65-DNA binding activity in IMR32 cells. As expected, the binding of nuclear NF-kB p65 to consensus oligonucleotide sequences was significantly increased 30 min following LPS challenge (Figure 9). Pre-treatment of IMR32 cells with the three different compounds for 24 h prevented the LPS-induced NF-kB p65 binding to consensus DNA sequences, reaching the maximal effect with compound **3m** at 1 μM dose (Figure 9). A concentration-dependent inhibitory effect was evident for all the compounds (Figure 9). These results suggest that compounds **3h** and **3m** and reference compound **2a** could modulate a seizure-induced oxinflammatory condition through regulating the NF-κB p65 signaling pathway that is involved in epilepsy.[18]

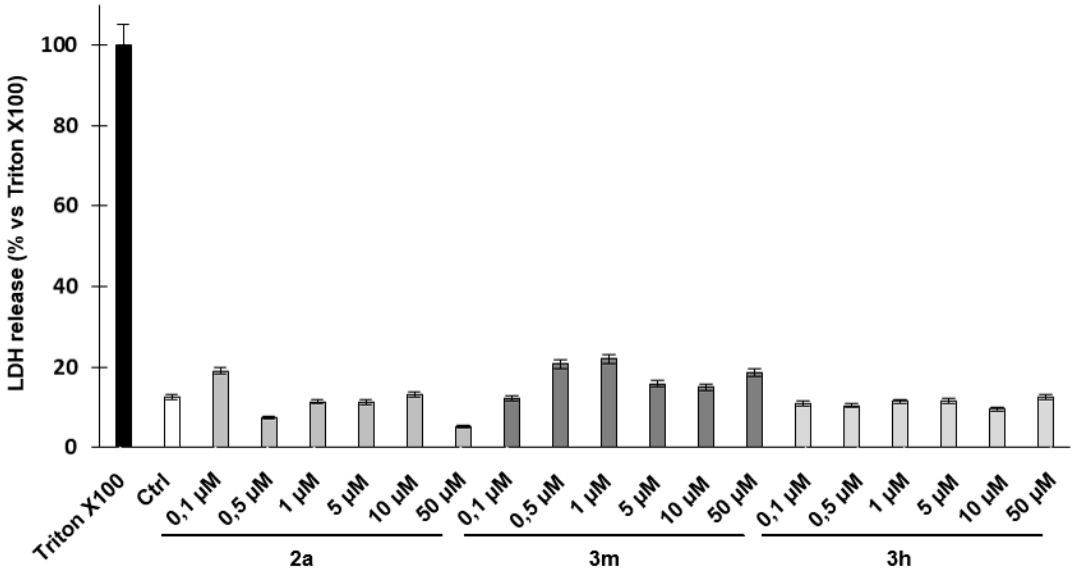

Figure 8. Cytotoxicity was determined as LDH release in IMR32 cells treated for 24 h with compounds **3h** and **3m** and reference compound **2a** at different concentrations (0.1, 0.5, 1, 5, 10 and 50 μM). Values represent the average +/- SD of samples performed at least in triplicate. Data

are expressed as a percentage of LDH release as compared to the maximum release of LDH from Triton X-100- treated cells (100%).

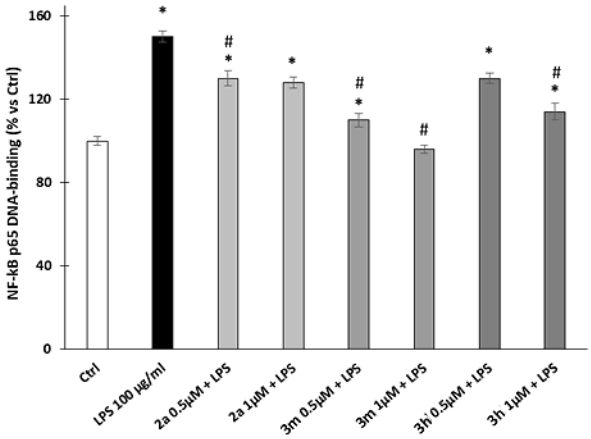

Figure 9. Effect of compounds **3m**, **3h** and **2a** on an oxinflammatory condition. NF-kB p65 DNA binding activity was evaluated in nuclear extracts from IMR32 cells pre-treated with compounds **3h** and **3m** and reference compound **2a** for 24 h and challenged with 100 µg/mL LPS for 30 min. Data are presented as mean ± SEM of 3 independent experiments. * p <0.05 vs Ctrl; # p <0.01 vs LPS treatment.

***In vivo* studies of 2a and 3h on rodent models of limbic epilepsy**

Effect of 2a on Maximal Dentate Activation (MDA), a model of partial complex epilepsy

MDA is a paroxysmal event characterized by the appearance of bursts of large amplitude population spikes in the dentate gyrus that is associated with the production of afterdischarges in limbic circuits. Repeated elicitation of MDA in the anesthetized rat produces a progressive increase in afterdischarge duration.[51-53] We have recently shown that CB manipulation significantly reduced the MDA elongation over the 4 h period of recording, with the CB1R/CB2R agonist WIN55,212-2 behaving differently from the FAAH inhibitor URB597 (**1**)

in terms of the magnitude of the effect and time-development.[54] The effects of the vehicle (n = 9) and **2a** treatment (n = 9) on the MDA paradigm are shown in Figure 10. An initial decrease in the time to onset (Figure 10A) was seen in vehicle-treated animals before leveling and remaining more constant. Treatment with **2a** had no significant effects on the time to onset of MDA and the graph followed the same pattern as with vehicle-treated animals. The duration of MDA (Figure 10B) saw a steady increase over time in vehicle-treated animals. Treatment with **2a** gave a reduction in the duration of MDA with significant effects 180 min after administration. The antiepileptic efficacy of **2a** during seizures in the MDA model was somewhat different from that observed with CB1R agonist and similar to that of the FAAH inhibitor URB597 (**1**).[54] Nevertheless, **2a** effect was appearing later than URB597 although, **2a** showed a stronger antiepileptic effect that improved over-time similar to another FAAH inhibitor AM374.[36] On the other hand, WIN55,212 affects MDA much faster, immediately following its administration.[54]

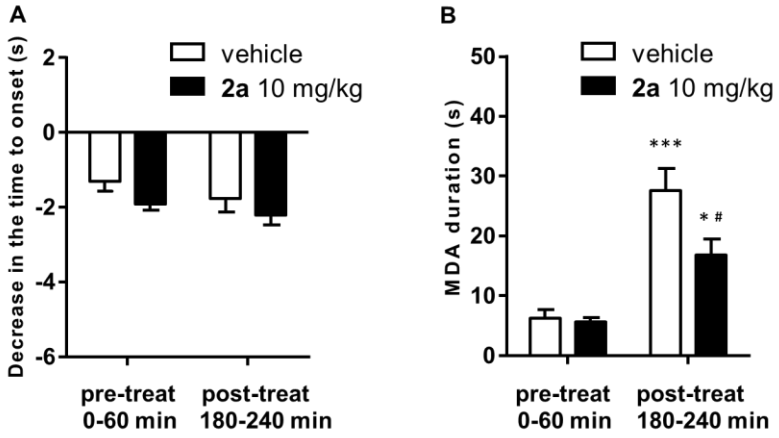

Figure 10. Maximal Dentate Activation (MDA) after tetanic stimulation of the perforant path (PP). (**A**) The time to onset of MDA decreased in both vehicle and **2a** treated animals with no significant difference between the two groups. (**B**) In vehicle-treated animals, the MDA duration increased over time, in animals treated with **2a** the increase in MDA duration was reduced from

180 mins post-treatment with effects up to 240 mins post-treatment. Repeated measures ANOVA followed by Bonferroni post hoc analysis, ***$p < 0.001$ *$p < 0.05$ vs pre-treatment, #$p < 0.05$ *vs* post-treatment.

Effect of 2a on hippocampal dentate gyrus long term potentiation (LTP)

Having demonstrated the anticonvulsant effect of the FAAH inhibitor **2a** in the MDA rat model of epilepsy, we next wanted to exclude any possible alteration of dentate gyrus excitability and plasticity in normal rats. Indeed, many exogenous cannabinoids such as WIN55,212-2 that have shown antiepileptic effects, showed negative effects on LTP,[54, 55] learning, and memory[32] that are already impaired in animal models of epilepsy.[54] We, therefore, performed electrophysiological recordings of the LTP at the level of the perforant path (PP)-dentate gyrus synapse of the hippocampus in anesthetized rats. In vehicle-treated animals (n = 9), high-frequency stimulation (HFS) current delivered to the PP resulted in potentiation shown by an increase in the population spike (PS) amplitude (Figure 12). The same potentiation was seen in animals (n = 4) given **2a** 30 mins before HFS and, at no point, was found a significant difference in PS amplitude (Figure 11) between the vehicle and **2a** groups. **2a** does not affect LTP similarly to **1** in normal conditions[54] and therefore, in people with epilepsy, it would be antiepileptic without exacerbating comorbid memory impairment.

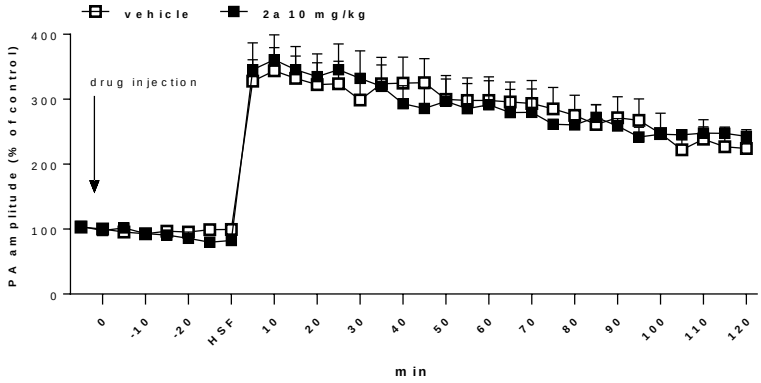

Figure 11. Effect of high-frequency stimulation (HFS) on long-term potentiation (LTP) in animals treated with vehicle or **2a**. In vehicle-treated animals, there was a large increase in the population spike (PS) amplitude. Animals treated with **2a** also exhibited the same effects with no significant difference between the vehicle-treated animals.

Effect of 2a pilocarpine-induced seizures, a model of limbic status epilepticus (SE)

Status epilepticus (SE) is a life-threatening condition characterized by continuous seizures with serious long-term consequences, such as neuronal death and the development of TLE.[56] We have recently shown that 2 mg/kg WIN55,212-2 decreased behavioral seizure severity of pilocarpine-induced SE in CB1R-dependent mechanism.[57, 58] Additionally, blockade of the FAAH alleviated behavioral, but not electrographic SE induced by kainic acid.[59, 60] Here we tested whether different doses of **2a** (2, 5 and 10 mg/kg, i.p.) were able to affect pilocarpine-induced SE (Figure 12).

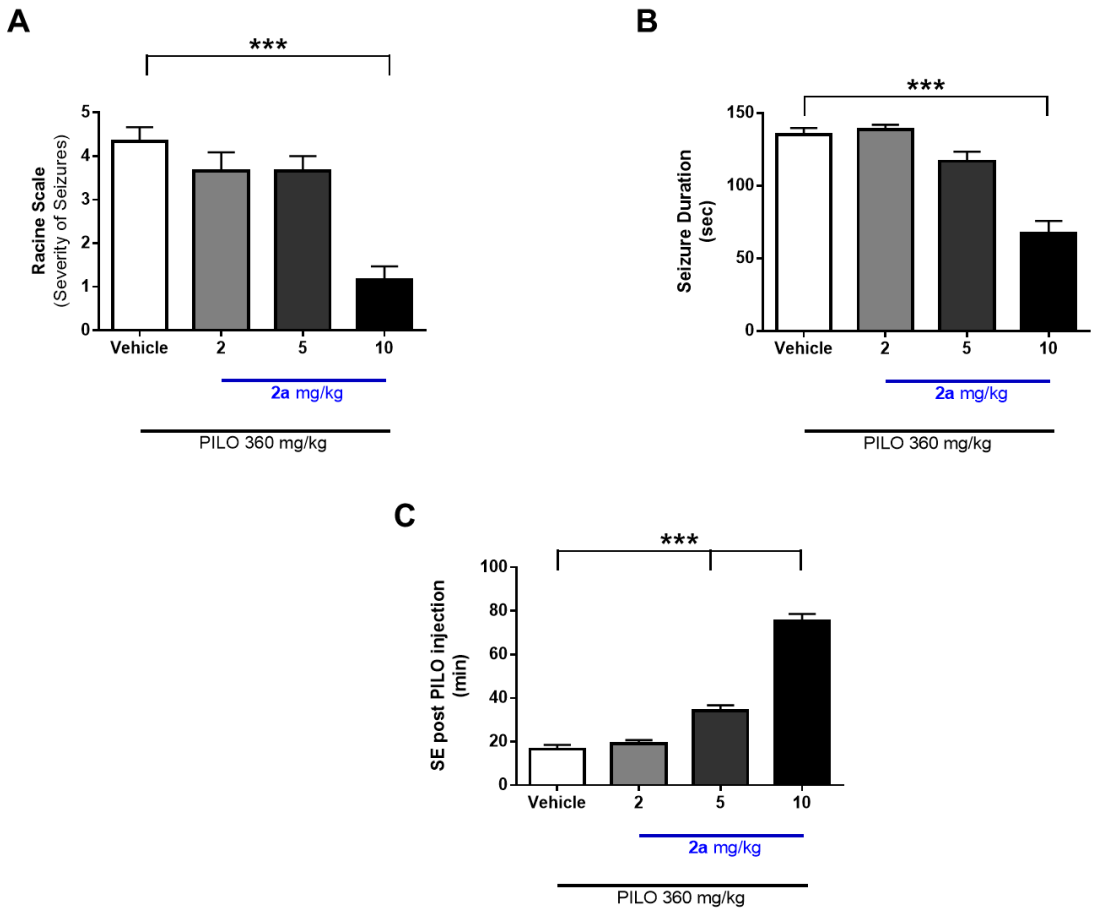

Figure 12. Effects of **2a** on pilocarpine-induced SE. (**A**) A dose of 10 mg/kg **2a** reduced the severity of seizures and (**B**) the duration of seizures compared to all other doses. No other dose had any significant effect on seizure severity or duration. (**C**) 10 mg/kg **2a** increased the time to onset of SE compared with vehicle. 2 and 5 mg/kg doses, and a dose of 5 mg/kg, increased the time to onset of SE compared to vehicle and 2 mg/kg dose. 1-way ANOVA with Bonferroni's Multiple Comparison ***$p < 0.005$.

Animals treated with vehicle (n = 6) after pilocarpine had severe behavioral seizures (Racine scale: 4.33 ± 0.33) that were long-lasting (135 ± 4.73 sec) and had a short time to onset (16.5 ± 2.07 mins). Pre-treatment with 10 mg/kg (n = 6) **2a** significantly reduced the severity of seizures (Racine scale: 1.16 ± 0.31; $p < 0.05$ *vs* 0.2 and 5 mg/kg), the duration of seizures (67 ± 8.68; $p <$

0.05 *vs* 0.2 and 5 mg/kg) and also significantly increased the time to onset of SE (75.2 ± 3.42; $p < 0.05$ *vs* 0.2 and 5 mg/kg). A dose of 5 mg/kg (n = 6) **2a** significantly increased the time to onset of SE compared with vehicle, while a dose of 2 mg/kg (34.1 ± 2.62 $p < 0.05$ *vs* 0.2 and 5 mg/kg) had no significant effect on seizure severity or duration. Similarly, the dose of 2 mg/kg had no significant effects on any seizure measurement.

Effect of 2a on hippocampal Thiol Oxidation labelling

Cannabinoids showed neuroprotective effects against oxidative damage in pilocarpine-induced SE[58, 61] in line with the suggestions that they can give protection against neurological damage.[29]

Here, we showed that **2a** affected histological thiol staining in the DG hippocampus 24 h after the pilocarpine administration. Representative images of the differential labeling of thiols are shown in Figure 13 panel A. A lighter shade of green indicates an increase in oxidized thiol and lighter red an increase in reduced thiol. Therefore, in the merged image, more green shades indicate higher oxidized thiols (vehicle, 2 and 5 mg/kg **2a**) whereas, the orange shades signify a lower amount (vehicle and 10 mg/kg **2a**). Ratiometric histochemistry analysis was performed to analyse these results quantitatively with total thiol oxidation compared against vehicle-treated animals (Figure 13 panel B). In animals treated 24 h before with pilocarpine, there was a significant increase in oxidized thiols (261 ± 13.8%; $p < 0.05$). There was still a significant increase in oxidized thiols in animals pre-treated (15 min before pilocarpine) with **2a** doses of 2 mg/kg (268 ± 5.7%; $p < 0.05$) or 5 mg/kg (273 ± 9.9%; $p < 0.05$). However, when pre-treated with 10 mg/kg **2a** there was no significant increase in the amount of thiol oxidation in the DG. During epileptic seizures, a vicious cycle (i.e. oxinflammation) starts as the seizure-mediated oxidative damage triggers the activation of redox-responsive transcription factors including NF-kB that, in turn, lead to boost the oxinflammatory state by producing and releasing other oxidant

species and inflammatory factors.[17, 18, 62] The FAAH inhibitor **2a** demonstrated anti-oxinflammatory by counteracting the loss of reduced thiols in the pilocarpine model of SE and could also prevent the activation of the NF-kB pathway. In this regard, the depletion of the cellular antioxidant pool of thiols is not just a mere index of oxidative damage caused by the SE but should be considered as a molecular event able to induce the NF-kB pathway, increasing the seizure susceptibility.[18]

In summary, preventing the oxinflammatory cycle could in part contribute to the overall antiepileptic efficacy of FAAH inhibitors.

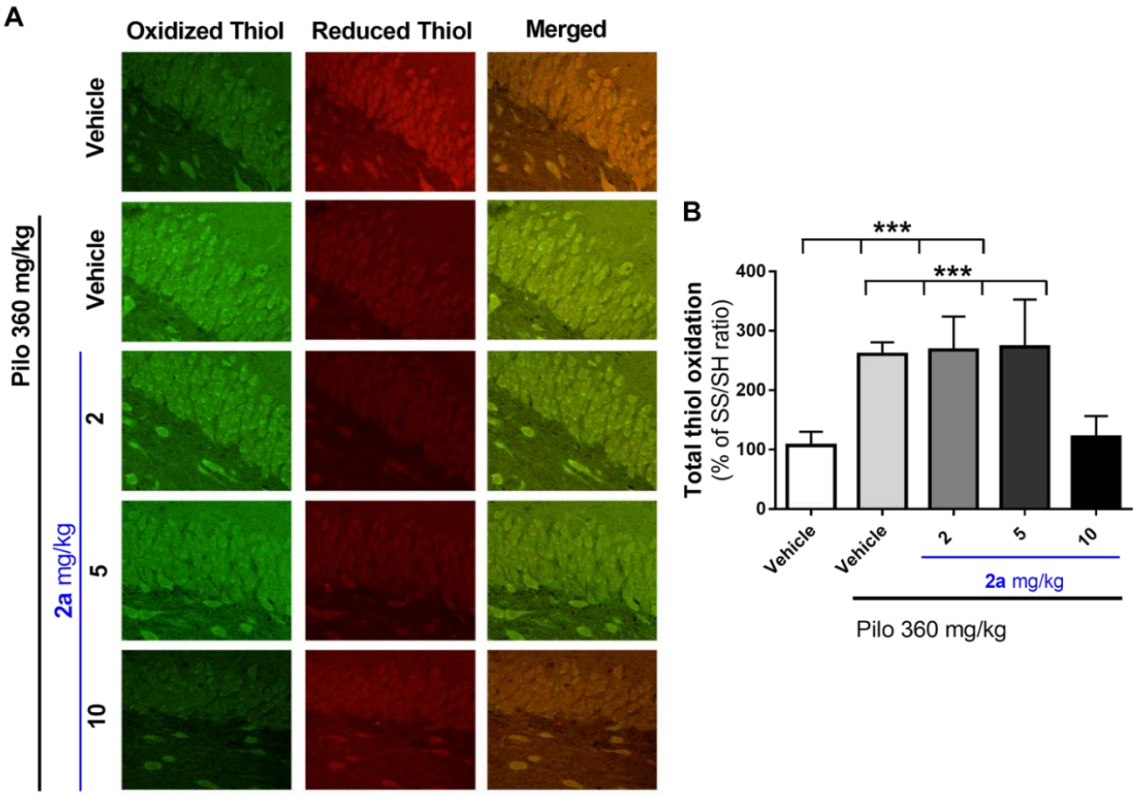

Figure 13. Thiol oxidation in the dentate gyrus of pilocarpine treated rats. (**A**) Differential labeling of total thiols in the Dentate Gyrus. Increased oxidized thiols can be observed in vehicle and doses of 2 and 5 mg/kg **2a** given after PILO. A dose of 10 mg/kg **2a** shows less oxidized thiols compared to other doses. (**B**) Ratiometric histochemistry analysis of thiols. Animals

treated with PILO showed significant thiol oxidation compared with vehicle-treated controls. Animals pre-treated with a dose of 10 mg/kg did not show this thiol oxidation. 1-way ANOVA followed by Tukey's Multiple Comparison Test; ***$p < 0.005$.

Effect of 3h on pilocarpine-induced seizures, a model of limbic status epilepticus (SE)

The encouraging results obtained with **2a** prompted us to further explore this series of FAAH inhibitors by using a medicinal chemistry approach. A systematic SAR analysis around a series of phenylpyrrole-based FAAH inhibitors, together with a combination of biochemical and biological studies, allowed the selection of **3h** as a suitable candidate for *in vivo* studies. Here we tested whether different doses of **3h** (2, 5 and 10 mg/kg, i.p.) were able to affect pilocarpine-induced SE (Figure 14) similarly to **2a**. Animals treated with vehicle (n = 6), after pilocarpine, had severe behavioral seizures (Racine scale: 4.16 ± 0.3), that were long-lasting (155 ± 5.52 sec) and had a short time to onset (29.3 ± 5.48 mins). Pre-treatment with 10 mg/kg (n = 6) **3h** significantly reduced the severity of seizures (Racine scale: 1 ± 0.36; $p < 0.005$), the duration of seizures (75 ± 15.06; $p < 0.01$), and also significantly increased the time to onset of SE (90.6 ± 7.83 $p < 0.005$). The dose of 5 mg/kg (n = 6) **3h** significantly reduced the duration of seizures (96 ± 16.42; $p < 0.05$) and increased the time to onset of SE compared with vehicle (69.3 ± 10.82 $p < 0.01$) however, had no significant effect on seizure severity or duration. Similar to **2a,** the dose of 2 mg/kg **3h** had no significant effects on any seizure measurement.

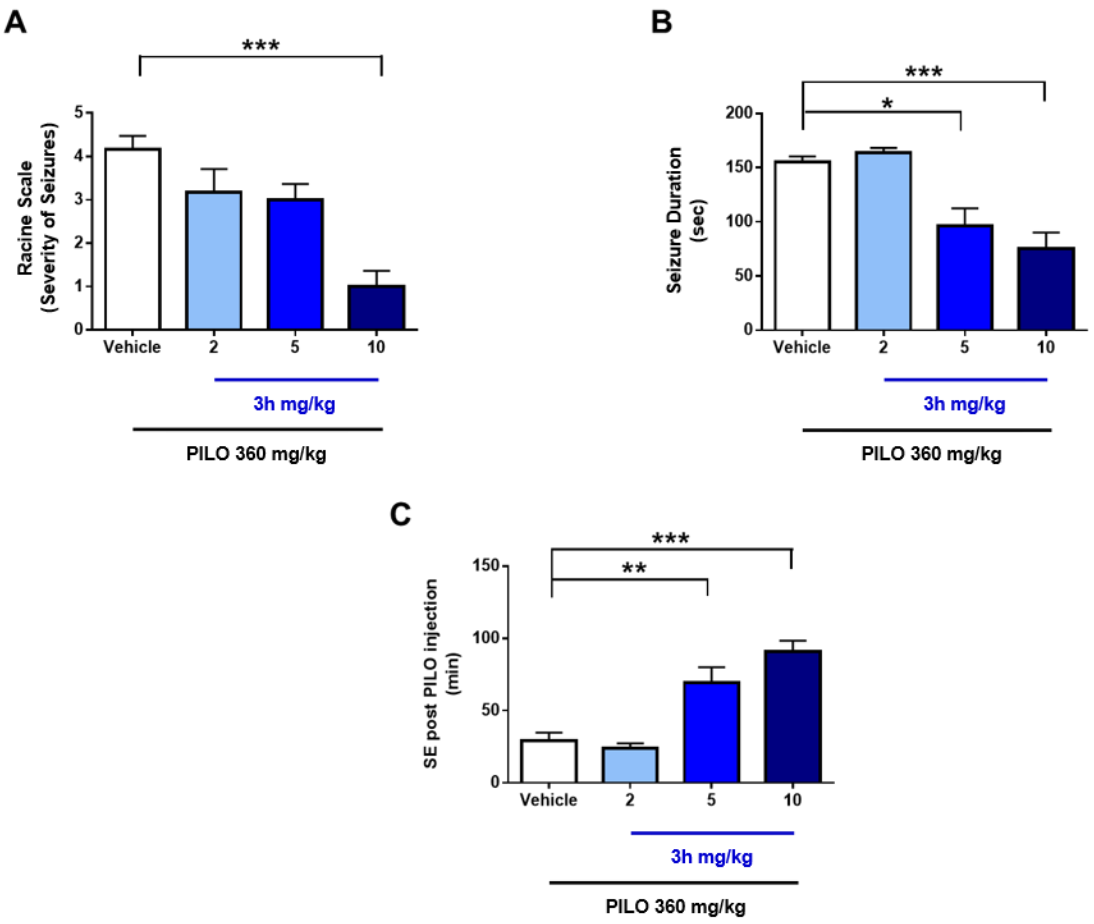

Figure 14. Effects of **3h** on pilocarpine-induced SE. (**A**) A dose of 10 mg/kg **3h** reduced the severity of seizures and (**B**) 5 and 10 mg/kg decreased the duration of seizures compared against all other doses. (**C**) 5 and 10 mg/kg **3h** increased the time to onset of SE compared with the vehicle and 2 mg/kg dose. 1-way ANOVA with Bonferroni's Multiple Comparison ***$p <$ 0.005, **$p < 0.01$, **$p < 0.05$

So far the use of different FAAH inhibitors has yielded varying but promising results in terms of their anti-epileptic properties,[36, 54, 63, 64] their neuroprotective qualities in protecting against excitotoxicity,[65] and also on their effect on LTP and memory.[37] In conclusion, the newly

synthesized FAAH inhibitor **2a** and **3h** display antiepileptic effects likely without impairing LTP and providing protection against oxidative damage caused by seizures.

Conclusions

The ECS can delay or prevent excitotoxic damage by modulating mitochondrial function and fine-tuning the excitatory/inhibitory stimuli. These effects can prevent OS-related epileptogenesis. On these bases, we have herein explored the effect of an indirect activation of the ECS in epilepsy. When we interrogated the effects of potent and selective FAAH inhibitors, such as our lead **2a** and the new inhibitor **3h**, in rodent models of epilepsy, they demonstrated promising activities. Our initial studies proved the efficacy of **2a** in the pilocarpine and the maximal dentate activation rat models of TLE during seizures and also using it as a pretreatment. These results demonstrated the positive effects on synaptic plasticity (short-term and long-term plasticity STP-LTP) and neuronal damages resulting from seizures (histological study of thiols formations). Based on these outcomes, we accomplished a further medicinal chemistry approach for identifying innovative compounds for the potential treatment of epilepsy. A systematic chemical expansion and SAR analysis around a new series of phenylpyrrole-based FAAH inhibitors (**3a-m**), flanked by a combination of biochemical and biological studies, allowed the selection of **3h** as a suitable candidate for *in vivo* studies. In brief, for compounds **3g**, **3m**, and **3h** we demonstrated selectivity over CB1R, CB2R and the MAGL enzyme. The safety profile of **3h** was ascertained by combining metabolic stability studies with cytotoxicity studies and the Ames test. Notably compounds **3h** and **3m** also demonstrated a potential anti-oxinflammatory profile on the neuroblastoma IMR32 cell line being able of decreasing the LPS-induced activation of NF-kB p65. The absence of cardiac toxicity was also ascertained for **3h**. Gratifyingly, when

tested *in vivo*, the new analogue **3h** replicated the antiepileptic potential of **2a** in the pilocarpine model, confirming the notable potential for this class of analogues against seizures.

Experimental section

Chemistry

All reagents were purchased from commercial suppliers and used without further purification. All moisture-sensitive reactions were performed under argon or nitrogen atmosphere using oven-dried glassware and anhydrous solvents. Dry tetrahydrofuran (THF) was freshly distilled from sodium/benzophenone while dichloromethane (DCM) and *N,N*-dimethylformamide (DMF) was freshly distilled from calcium hydride and stored under argon atmosphere. Flash column chromatography was carried out on silica gel (Merck: Kieselgel 60, particle size 0.040–0.063 mm). Reverse phase column chromatography was carried out on Lichroprep RP-18 (25-40 μm, Merck). Reactions' progression was monitored by thin-layer chromatography (TLC), carried out using glass-backed plates coated with Merck Kieselgel 60 GF254. Plates were visualized under UV light (at 254 nm) or by staining with potassium permanganate, ninhydrin, or cerium ammonium molybdate followed by heating. MW reactions were performed in a Discovery Microwave System (CEM). ^{1}H NMR and ^{13}C NMR spectra were recorded on a Varian 300 MHz, or a Bruker 400 MHz spectrometer using the residual signal of the deuterated solvent as an internal standard. Coupling constant (J) are given in Hz. Splitting patterns are described as singlet (s), doublet (d), triplet (t), quartet (q), and broad (br); the value of chemical shifts (δ) are given in ppm. Mass spectra were recorded utilizing electron spray ionization (ESI) Agilent 1100 Series LC/MSD spectrometer. Yields refer to purified products and are not optimized. All

compounds that were tested in the biological assays were analyzed by combustion analysis (CHN) to confirm the purity >95%.

6-Phenylhexyl (3-(3-cyano-1*H*-pyrrol-1-yl)phenyl)carbamate (6a). To a 0 °C cooled solution of **4** (80 mg, 0.44 mmol) and dry pyridine (89 µL, 1.1 mmol) in dry DCM (8 mL), a solution of phosgene (20% in toluene, 279 µL, 0.53 mmol) was added. The reaction was warmed to 25 °C and stirred for 5 h affording *1-(3-isocyanatophenyl)-1H-pyrrole-3-carbonitrile*; ESI-MS *m/z*: 242 $[M+Na]^+$. After this time a solution of **5a** (94.5 mg, 0.53 mmol) in dry DCM (10.0 mL) was added. The resulting mixture was stirred for 20 h at 25 °C Evaporation and silica gel column chromatography (0-5% EtOAc in DCM) gave the title compound as a pale oil (yield 46%). ESI-MS *m/z*: 410 $[M+Na]^+$. ^{1}H NMR (400 MHz, $CDCl_3$) δ 7.70 (br s, 1H), 7.49 – 7.46 (m, 1H), 7.35 – 7.32 (m, 4H), 7.30 (d, *J* = 7.6 Hz, 1H), 7.29 – 7.25 (m, 3H), 7.22 – 7.13 (m, 1H), 7.03 – 6.94 (m, 1H), 6.55 (dd, *J* = 3.0, 1.6 Hz, 1H), 4.29 – 4.10 (m, 2H), 2.67 – 2.52 (m, 2H), 1.74 – 1.54 (m, 4H), 1.47 – 1.29 (m, 4H).

2-(2-Phenoxyethoxy)ethyl (3-(3-cyano-1*H*-pyrrol-1-yl)phenyl)carbamate (6b). The title compound was prepared according to the procedure described for **6a** starting from **4** (80 mg, 0.44 mmol) and **5b** (96.5 mg, 0.53 mmol). Alumina column chromatography (30-100% Et_2O in petroleum ether) gave title compound as a pale yellow oil (yield 33%). ESI-MS *m/z*: 414 $[M+Na]^+$. ^{1}H NMR (300 MHz, $CDCl_3$) δ 7.66 (br s, 1H), 7.46 (d, *J* = 0.4 Hz, 1H), 7.33 (t, *J* = 8.1 Hz, 1H), 7.29 – 7.21 (m, 2H), 7.19 – 7.12 (m, 2H), 7.04 – 6.98 (m, 2H), 6.94 – 6.86 (m, 3H), 6.56 – 6.51 (m, 1H), 4.42 – 4.25 (m, 2H), 4.17 – 4.04 (m, 2H), 3.90 – 3.81 (m, 4H).

2-(2-(4-Fluorophenoxy)ethoxy)ethyl (3-(3-cyano-1*H*-pyrrol-1-yl)phenyl)carbamate (6c). The title compound was prepared according to the procedure described for **6a**, starting from **4** (80 mg, 0.44 mmol) and **5c** (106.1 mg, 0.53 mmol). Evaporation and alumina column

chromatography (25-100% Et_2O in petroleum ether) afforded title compound as a pale yellow oil (14% yield). ESI-MS *m/z*: 432 $[M+Na]^+$, 448 $[M+K]^+$. ^1H NMR (300 MHz, $CDCl_3$) δ 7.69 (br s, 1H), 7.49 (t, *J* = 1.9 Hz, 1H), 7.35 (t, *J* = 8.1 Hz, 1H), 7.18 – 7.11 (m, 1H), 7.07 – 7.00 (m, 2H), 6.98 – 6.90 (m, 3H), 6.88 – 6.79 (m, 2H), 6.56 (s, 1H), 4.52 – 4.28 (m, 2H), 4.15 – 4.06 (m, 2H), 3.88 – 3.81 (m, 4H).

2-(2-(2-Fluorophenoxy)ethoxy)ethyl (3-(3-cyano-1*H*-pyrrol-1-yl)phenyl)carbamate (6d). The title compound was prepared according to the procedure described for **6a**, starting from **4** (80 mg, 0.44 mmol) and **5d** (106.1 mg, 0.53 mmol). Evaporation and silica gel column chromatography (0-5% EtOAc in DCM) afforded title compound as a pale yellow oil. (55% yield). ESI-MS *m/z*: 432 $[M+Na]^+$. ^1H NMR (400 MHz, $CDCl_3$) δ 7.66 (br s, 1H), 7.45 (d, *J* = 1.5 Hz, 1H), 7.32 (t, *J* = 8.1 Hz, 1H), 7.17 – 7.11 (m, 1H), 7.04 – 6.91 (m, 6H), 6.90 – 6.83 (m, 1H), 6.56 – 6.49 (m, 1H), 4.40 – 4.32 (m, 2H), 4.22 – 4.15 (m, 2H), 3.90 – 3.86 (m, 2H), 3.83 – 3.78 (m, 2H).

6-Phenylhexyl (3-(3-carbamoyl-1*H*-pyrrol-1-yl)phenyl)carbamate (3a). To a solution of **6a** (65 mg, 0.17 mmol) in 1,4-dioxane (12 mL), sodium perborate tetrahydrate (99 mg, 0.65 mmol) in H_2O (12 mL) was added. Reaction mixture was heated to 80 °C for 20 h. After cooling to 25 °C, the reaction mixture was diluted with distilled H_2O (10 mL) and extracted with EtOAc (3 x 10 mL). The combined organic layers were washed with a saturated solution of NaCl, dried over anhydrous sodium sulphate, filtered and concentrated. Column chromatography (0-5% MeOH in DCM) afforded the title compound as an amorphous white solid (25% yield) ESI-MS *m/z*: 428 $[M+Na]^+$.^1H NMR (300 MHz, acetone-d_6) δ 8.87 (br s, 1H), 7.90 (s, 1H), 7.79 (s, 1H), 7.52 – 7.35 (m, 3H), 7.31 – 7.16 (m, 6H), 6.97 (s, 1H), 6.73 (br s, 1H), 6.21 (br s, 1H), 4.14 (t, *J* = 6.5 Hz, 2H), 2.61 (t, *J* = 7.6 Hz, 2H), 1.76 – 1.33 (m, 8H). ^{13}C NMR (75 MHz, acetone-d_6) δ 165.5,

153.9, 142.8, 141.1, 140.8, 130.4, 130.3, 128.5, 128.4, 125.8, 122.5, 121.7, 120.7, 120.1, 116.2, 114.6, 114.3, 110.4, 35.7, 31.5, 29.4, 29.0, 28.9, 25.7. Anal. ($C_{24}H_{27}N_3O_3$) C, H, N.

2-(2-Phenoxyethoxy)ethyl (3-(3-carbamoyl-1*H*-pyrrol-1-yl)phenyl)carbamate (3b). Starting from **6b** (56 mg, 0.14 mmol), the title compound was obtained following the same procedure described for **3a**. Silica gel column chromatography (0-5% MeOH in DCM) afforded title compound as an amorphous white solid. (25% yield). ESI-MS *m/z*: 410 $[M+H]^+$, 432 $[M+Na]^+$. ^{1}H NMR (300 MHz, acetone-d_6) δ 8.99 (br s, 1H), 7.90 (t, J = 2.0 Hz, 1H), 7.79 (t, J = 1.8 Hz, 1H), 7.53 – 7.36 (m, 2H), 7.33 – 7.14 (m, 4H), 7.00 – 6.84 (m, 3H), 6.79 – 6.67 (m, J = 2.7, 1.7 Hz, 1H), 6.78 – 6.66 (m, 1H), 6.20 (br s, 1H), 4.35 – 4.27 (m, 2H), 4.18 – 4.11 (m, 2H), 3.90 – 3.76 (m, 4H). ^{13}C NMR (75 MHz, acetone-d_6) δ 166.3, 165.4, 159.2, 153.7, 141.1, 140.8, 130.3, 129.6, 122.5, 121.7, 120.8, 120.1, 117.1, 116.2, 114.7, 114.4, 110.4, 110.2, 69.6, 69.4, 67.5, 64.2. Anal. ($C_{22}H_{23}N_3O_5$) C, H, N.

2-(2-(4-Fluorophenoxy)ethoxy)ethyl (3-(3-carbamoyl-1*H*-pyrrol-1-yl)phenyl)carbamate (3c). Starting from **6c** (25 mg, 0.06 mmol), the title compound was obtained following the procedure described for **3a**. The crude was purified by column chromatography on silica gel (0-5% MeOH/DCM) affording pure compound **3c** as an amorphous white solid. (25% yield). ESI-MS *m/z*: 450 $[M+Na]^+$. ^{1}H NMR (300 MHz, acetone-d_6) δ 8.95 (br s, 1H), 7.90 (s, 1H), 7.78 (t, J = 1.9 Hz, 1H), 7.52 – 7.36 (m, 2H), 7.28 – 7.16 (m, 2H), 7.11 – 6.89 (m, 4H), 6.79 – 6.69 (m, 1H), 6.40 – 5.94 (m, 2H), 4.37 – 4.25 (m, 2H), 4.20 – 4.05 (m, 2H), 3.87 – 3.82 (m, 2H), 3.81 – 3.77 (m, 2H). ^{13}C NMR (75 MHz, acetone-d_6) δ 165.7, 165.3, 157.2, 153.7, 141.0, 140.8, 130.3, 121.6, 120.9, 120.0, 116.2, 116.0, 115.9, 115.9, 115.6, 115.5, 114.5, 113.6, 69.6, 69.4, 68.3, 64.2. Anal. ($C_{22}H_{22}FN_3O_5$) C, H, N.

2-(2-(2-Fluorophenoxy)ethoxy)ethyl (3-(3-carbamoyl-1*H*-pyrrol-1-yl)phenyl)carbamate (3d). Starting from **6d** (50 mg, 0.12 mmol), the title compound was obtained following the same procedure described for **3a**. Silica gel column chromatography (0-2% MeOH in DCM) afforded pure compound **3d** as an amorphous white solid. (25% yield). ESI-MS *m/z*: 450 $[M+Na]^+$. ^1H NMR (300 MHz, acetone-d_6) δ 8.96 (br s, 1H), 7.90 (s, 1H), 7.78 (s, 1H), 7.54 – 7.33 (m, 3H), 7.20 (t, *J* = 12.6 Hz, 3H), 7.09 (t, *J* = 7.8 Hz, 2H), 6.93 (br s, 1H), 6.73 (s, 1H), 6.36 – 5.94 (m, 1H), 4.39 – 4.28 (m, 2H), 4.26 – 4.18 (m, 2H), 3.93 – 3.85 (m, 2H), 3.83 – 3.77 (m, 2H). ^{13}C NMR (75 MHz, acetone-d_6) δ 165.3, 153.7, 149.0, 141.0, 140.8, 130.3, 127.4, 124.8, 124.7, 121.6, 121.4, 121.3, 116.2, 116.0, 115.5, 114.5, 110.4, 110.2, 69.5, 69.4, 69.0, 64.2. Anal. ($C_{22}H_{22}FN_3O_5$) C, H, N.

1-(3-Aminophenyl)-1*H*-pyrrole-3-carboxamide (7). To a solution of **4** (65.0 mg, 0.35 mmol) in EtOH (22.0 mL), 6N NaOH (867.0 µL) and 30% H_2O_2 (867.0 µL) were added. The reaction mixture was refluxed for 3h. After cooling to 25 °C, a saturated solution of $Na_2S_2O_3$ (2.0 mL) was added and the solvent was evaporated under reduced pressure. The residue was taken up with H_2O and extracted with EtOAc (3 x 5 mL). The combined organic layers were washed with a saturated solution of NaCl, dried over anhydrous sodium sulphate, filtered and concentrated. The crude was used in the next step without any further purification (yellow solid, 90% yield). ESI-MS *m/z*: 224 $[M+Na]^+$. ^1H NMR (300 MHz, $CDCl_3$) δ 7.69 – 7.53 (m, 1H), 7.20 (t, *J* = 8.0 Hz, 1H), 7.03 – 6.94 (m, 1H), 6.82 – 6.73 (m, 1H), 6.68 (d, *J* = 2.1 Hz, 1H), 6.65 – 6.58 (m, 1H), 6.56 – 6.47 (m, 1H), 5.53 (br s, 2H), 3.82 (br s, 2H).

1-(3-(3-(6-Phenylhexyl)ureido)phenyl)-1*H*-pyrrole-3-carboxamide (3e). To a solution of **7** (30 mg, 0.15 mmol) in dry THF (5.0 mL), TEA (83.6 µL, 0.60 mmol) and 6-phenylhexan-1-yl-isocyanate (121 mg, 0.60 mmol) were sequentially added. The reaction mixture was stirred at 25

°C for 16 h. Evaporation and silica gel column chromatography (5% MeOH in DCM) gave the title compound as an amorphous white solid (62% yield). ESI-MS *m/z*: 405 $[M+H]^+$. ^{1}H NMR (300 MHz, acetone-d_6) δ 8.59 (br s, 1H), 7.81 – 7.69 (m, 2H), 7.43 (s, 1H), 7.36 – 6.97 (m, 8H), 6.82 (s, 1H), 6.65 – 6.56 (m, 1H), 6.66 – 6.57 (m, 1H), 6.21 (t, *J* = 5.6 Hz, 1H), 3.29 – 3.24 (m, 2H), 3.12 – 2.97 (m, 2H), 1.62 – 1.34 (m, 4H), 1.29 – 1.21 (m, 4H). ^{13}C NMR (75 MHz, DMSO) δ 165.7, 155.7, 142.9, 142.6, 140.5, 130.6, 128.9 (2), 128.9 (2), 126.3, 122.6, 121.9, 120.5, 116.0, 113.1, 110.9, 109.6, 35.8, 31.7, 31.6, 30.3, 29.1, 26.9. Anal. ($C_{24}H_{28}N_4O_2$) C, H, N.

3-(3-Cyano-1*H*-pyrrol-1-yl)-*N*-(6-phenylhexyl)benzamide (9). To a 0 °C cooled solution of **8** (200 mg, 0.94 mmol) and PPh_3 (495 mg, 1.95 mmol) in dry DCM (30.0 mL) hexachloroacetone (74 μL) was added and the reaction was stirred for 30 min. A solution of 6-phenylhexan-1-amine (111 mg, 0.63 mmol) and TEA (88 μL) in DCM (5.0 mL), prepared in a different flask, was added. The resulting mixture was stirred for an additional 1 h at 0 °C. After this time, saturated aqueous $NaHCO_3$ was added and the aqueous layer was extracted with DCM (3 x 10 mL). The combined organic layers were washed with a saturated solution of NaCl, dried over anhydrous sodium sulphate, filtered and concentrated. The crude was purified by column chromatography on silica gel (40% EtOAc in petroleum ether) affording the title compound as an amorphous white solid. (30% yield). ESI-MS *m/z*: 394 $[M+Na]^+$. ^{1}H NMR (300 MHz, $CDCl_3$) δ 7.86 (br s, 1H), 7.69 (d, *J* = 7.3 Hz, 1H), 7.59 – 7.42 (m, 3H), 7.30 – 7.02 (m, 6H), 6.59 (d, *J* = 1.2 Hz, 1H), 6.39 (s, 1H), 3.59 – 3.28 (m, 2H), 2.60 (t, *J* = 7.6 Hz, 2H), 1.73 – 1.49 (m, 4H), 1.40 (m, 4H).

1-(3-((6-Phenylhexyl)carbamoyl)phenyl)-1*H*-pyrrole-3-carboxamide (3f). Starting from **9** (85 mg, 0.23 mmol), the title compound was obtained following the same procedure described for **3a**. Column chromatography on silica gel (5% MeOH in DCM) afforded pure compound **3j**

as an amorphous white solid. (42% yield). ESI-MS *m/z*: 412 $[M+Na]^+$. ^{1}H NMR (300 MHz, acetone, d_6) δ 8.06 (br s, 1H), 7.98 (s, 1H), 7.89 – 7.78 (m, 2H), 7.74 – 7.69 (m, 1H), 7.64 – 7.54 (m, 5H), 7.38 – 7.11 (m, 1H), 7.08 – 6.90 (br s, 1H), 6.76 (br s, 1H), 6.33 (s, 2H), 3.48 – 3.28 (m, 2H), 2.65 – 2.41 (m, 2H), 1.71 – 1.52 (m, 4H), 1.49 – 1.33 (m, 4H). ^{13}C NMR (75 MHz, acetone-d_6), δ 165.6, 165.4, 142.9, 140.2, 137.2, 130.1, 128.5 (2C), 128.4 (2C), 125.7, 125.2, 122.8, 122.6, 121.9, 120.2, 118.9, 110.6, 39.9, 35.8, 31.6, 29.6, 28.9, 26.9. Anal. ($C_{24}H_{27}N_3O_2$) C, H, N.

1-(5-Methoxy-2-nitrophenyl)-1*H*-pyrrole-3-carbonitrile (11). To a solution of 5-methoxy-2-nitroaniline (2.0 g, 11.89 mmol) in 1,4-dioxane (114 mL), dimethoxytetrahydrofuran-3-carbonitrile **10** (2.2 g, 14.3 mmol) was added; the resulting mixture was refluxed for 20 min., then 11.8 mL of 6 M HCl were added dropwise and the reaction refluxed for further 20 min. After cooling to 25 °C, the solvent was removed under reduced pressure. The residue was suspended with H_2O (20 mL) and extracted with DCM (3 x 20 mL). The combined organic layers were washed with a saturated solution of NaCl, dried over anhydrous sodium sulphate, filtered and concentrated. The crude was purified by column chromatography on silica gel (20% EtOAc in petroleum ether) to afford **11** as an amorphous brown solid (87% yield). ESI-MS *m/z*: 244 $[M+H]^+$; 266 $[M+Na]^+$. ^{1}H NMR (300 MHz, $CDCl_3$) δ 8.10 (d, J = 9.2 Hz, 1H), 7.28 (dd, J = 2.2, 1.6 Hz, 1H), 7.06 (dd, J = 9.2, 2.7 Hz, 1H), 6.89 (d, J = 2.7 Hz, 1H), 6.76 (dd, J = 3.0, 2.3 Hz, 1H), 6.60 (dd, J = 3.0, 1.6 Hz, 1H), 3.94 (s, 3H).

1-(5-Hydroxy-2-nitrophenyl)-1*H*-pyrrole-3-carbonitrile (12). To a suspension of **11** (500 mg, 2,0 mmol) in dry DCM (20.0 mL), cooled at -78 °C, boron tribromide (1 M solution in DCM 20.0 mL)was added. The reaction mixture was warmed to 25 °C. and stirred for 96 h. The mixture was treated with 4M NaOH and extracted with DCM (3 x 15 mL); the aqueous layer was acidified to pH = 2 with 6M HCl and extracted with EtOAc (3 x 15 mL). The combined organic

extracts were dried over anhydrous sodium sulphate, filtered and concentrated under reduced pressure to afford **12** (50% yield). ESI-MS *m/z*: 228 [*M*-H]$^-$. ^{1}H NMR (400 MHz, acetone-d_6) δ 10.16 (s, 1H), 8.09 (d, *J* = 9.0 Hz, 1H), 7.66 (m, 1H), 7.12 (m, 1H), 7.03 (m, 2H), 6.60 (m, 1H).

1-(5-Hydroxy-2-nitrophenyl)-1*H*-pyrrole-3-carboxamide (13a). Starting from **12** (570 mg, 2,49 mmol), the title compound was prepared according to the procedure followed for **7**. Purification by flash chromatography on silica gel (0-5% MeOH in EtOAc), afforded the title compound as amorphous orange solid. (40% yield). ESI-MS *m/z*: 246 [*M*-H]$^-$. ^{1}H NMR (300 MHz, CD_3OD) δ 8.00 (d, *J* = 9 Hz, 1H), 7.43 (t, *J* = 2.1, 1H), 6.95 (dd, *J* = 9.3, 2.7 Hz, 1H), 6.86 (d, *J* = 2.7 Hz, 1H), 6.83 (t, *J* = 2.4, 1H), 6.70 – 6.68 (m, 1 H).

4-Amino-3-(3-carbamoyl-1*H*-pyrrol-1-yl)phenyl (6-phenylhexyl)carbamate (3g). To a solution of **13a** (134 mg, 0,54 mmol) in dry toluene (12.0 mL) and dry DMF (3.0 mL), 6-phenylhexan-1-yl-isocyanate(219 mg, 1.08 mmol) and TEA (9 µL, 0.06 mmol) were sequentially added. The reaction mixture was refluxed for 48 h. After cooling to 25 °C, solvents were removed *in vacuo*. The residue was immediately dissolved in EtOH (10 mL), and a catalytic amount of 10% Pd/C was added. The reaction mixture was stirred at 25 °C under H_2 atmosphere for 4 h. Thereafter, the Pd/C was filtered off and EtOH was evaporated under reduced pressure. Silica gel column chromatography (100% EtOAc) gave the title compound as colorless oil (45% yield). ESI-MS *m/z*: 421 [*M*+H]$^+$. ^{1}H NMR (300 MHz, acetone-d_6) δ 7.43 (t, *J* = 1.9 Hz, 1H), 7.31 – 7.10 (m, 5H), 6.97 – 6.82 (m, 5H), 6.69 (dd, *J* = 2.9, 1.7 Hz, 2H), 6.23 (br s, 1H), 4.50 (br s, 2H), 3.20 – 3.16 (m2H), 2.61 (t, *J* = 7.7 Hz, 2H), 1.68 – 1.48 (m, 4H), 1.48 – 1.25 (m, 4H). ^{13}C NMR (75 MHz, acetone-d_6) δ 165.6, 155.1, 142.9, 142.7, 140.4, 128.5 (2), 128.54 (2), 128.4, 125.9, 125.7, 124.2, 122.5, 121.6, 120.1, 116.3, 109.6, 41.0, 35.8, 29.8, 28.9, 31.6, 26.6. Anal. ($C_{24}H_{28}N_4O_3$) C, H, N.

3-(3-Carbamoyl-1*H*-pyrrol-1-yl)phenyl (2-(4-benzylpiperazin-1-yl)ethyl)carbamate (3k). To a solution of **13b** (30 mg, 0.15 mmol) and DMAP (73 mg, 0.60 mmol) in dry THF (12 mL) cooled to 0 °C a solution of phosgene (20% in toluene, 157 μL, 0.3 mmol) was added. The reaction mixture was warmed to 25 °C and stirred for 30 min under N_2 atmosphere. At this time the amine **14** (65 mg, 0.30 mmol) was added. The resulting mixture was refluxed for 16 h. After the evaporation and purification by silica gel column chromatography (2-5% MeOH in AcOEt) the title compound was obtained as an amorphous white solid. (20% yield). ^{1}H NMR (300 MHz, $CDCl_3$): δ 7.64 (s, 1H), 7.41 (t, *J* = 8.30 Hz, 1H), 7.33-7.21 (m, 7H), 7.09 (d, *J* = 8.68 Hz, 1H), 7.02 (s, 1H), 6.55 (s, 1H), 5.86 (brs, 1H), 5.60 (brs, 2H), 3.56 (s, 2H), 3.40 (d, *J* = 5.27 Hz, 2H), 2.59 (br s, 10H). ^{13}C NMR (75 MHz, $CDCl_3$): δ 166.1, 154.1, 151.9, 140.5, 130.4, 129.31, 128.31, 127.31, 122.6, 120.6, 119.9, 117.5, 114.6, 109.6, 62.7, 56.6, 52.6, 37.4, 29.7. Anal. ($C_{25}H_{29}N_5O_3$) C, H, N.

3-(3-Carbamoyl-1,5-dimethyl-1*H*-pyrrol-2-yl)phenyl (6-phenylhexyl)carbamate (3h). To a solution of **15a** (30 mg, 0.13 mmol) in dry THF, 6-phenylhexan-1-yl-isocyanate (53 mg, 0.26 mmol) and TEA (72 μL, 0.52 mmol) were sequentially added. The resulting mixture was refluxed for 12 h. After cooling to 25 °C and after evaporation, silica gel column chromatography (2% MeOH in DCM) afforded the title compound as pale-yellow oil. (36% yield). ESI-MS *m/z*: 434 $[M+H]^+$, 456 $[M+Na]^+$. ^{1}H NMR (300 MHz, $CDCl_3$) δ 7.45 (t, *J* = 7.5 Hz, 1H), 7.29-7.15 (m, 8H), 6.43 (s, 1H), 5.20 (br s, 3H), 3.26 (s, 3H), 3.24-3.20 (m, 2H), 2.60 (t, *J* = 7.5 Hz, 2H), 2.23 (s, 3H), 1.65-1.56 (m, 4H), 1.39-1.35 (m, 4H). ^{13}C NMR (75 MHz, $CDCl_3$) δ 166.9, 154.5, 151.6, 142.8, 133.3, 133.2, 130.1, 129.7 (2C), 128.6 (2C), 128.5, 127.9, 125.9, 124.6, 122.4, 115.7, 108.2, 41.5, 36.1, 31.7, 31.5, 29.9, 29.1, 26.1. Anal. ($C_{26}H_{31}N_3O_3$) C, H, N.

3-(3-Carbamoyl-5-methyl-1*H*-pyrrol-2-yl)phenyl (6-phenylhexyl)carbamate (3i). Starting from **15b** (30 mg, 0.14 mmol), 6-phenylhexan-1-yl-isocyanate (57 mg, 0.28 mmol) and TEA (77 μL, 0.56 mmol), the title compound was prepared according to the procedure followed for **3h**. Column chromatography on silica gel (1% MeOH in DCM), affording **3i** as an amorphous white solid (20% yield). ESI-MS *m/z*: 442 $[M+Na]^+$, 458 $[M+K]^+$. ^{1}H NMR (300 MHz, $CDCl_3$) δ 8.40 (br s, 1H), 7.40-7.34 (m, 2H), 7.29-7.24 (m, 3H), 7.18-7.15 (m, 3H), 7.08-7.06 (m, 1H), 6.28 (s, 1H), 5.35 (br s, 1H), 5.25 (brs, 1H), 5.15 (brs, 1H), 3.26-3.19 (m, 2H), 2.61 (t, *J* = 7.2 Hz, 2H), 2.24 (s, 3H), 1.65-1.56 (m, 4H), 1.39-1.35 (m, 4H). ^{13}C NMR (75 MHz, $CDCl_3$) δ 167.4, 154.8, 151.4, 142.8, 133.5, 131.6, 129.9, 128.6 (2C), 128.5 (2C), 128.4, 125.9, 122.3, 121.4, 115.8, 108.9, 41.5, 36.1, 31.5, 29.9, 29.1, 26.8, 12.9. Anal. ($C_{25}H_{29}N_3O_3$) C, H, N.

3-(5-Carbamoyl-1-methyl-1*H*-pyrrol-2-yl)phenyl (6-phenylhexyl)carbamate (3j). Starting from **16** (35 mg, 0.16 mmol), the title compound was prepared according to the procedure followed for **3h**. Silica gel column chromatography (2% MeOH in DCM) afforded **3j** as colourless oil (79% yield). ESI-MS *m/z*: 442 $[M+Na]^+$. ^{1}H NMR (300 MHz, $CDCl_3$) δ 7.40 (t, *J* = 7.2 Hz, 1H), 7.30-7.13 (m, 8H), 6.67 (d, *J* = 3.3 Hz, 1H), 6.18 (d, *J* = 4.2 Hz, 1H), 5.70 (br s, 2H), 5.18 (br s, 1H), 3.89 (s, 3H), 3.29-3.22 (m, 2H), 2.62 (t, *J* = 7.2 Hz, 2H), 1.66-1.55 (m, 4H), 1.43-1.39 (m, 4H).^{13}C NMR (75 MHz, $CDCl_3$) δ 164.1, 154.6, 151.3, 142.8, 140.1, 133.6, 129.5, 128.6 (2C), 128.5 (2C), 126.3, 126.3, 125.9, 122.8, 121.4, 113.3, 109.0, 41.5, 36.1, 34.8, 31.6, 30.0, 29.1, 26.8. Anal. ($C_{25}H_{29}N_3O_3$) C, H, N.

3-(1*H*-Pyrrol-1-yl)phenol (18). A solution of 3-aminophenol (100 mg, 0.91 mmol) and 2,5-dimethoxytetrahydrofuran **17** (145 mg, 1.09 mmol) in AcOH (1.0 mL) was placed in a sealed tube and heated to 170 °C in a microwave apparatus to a power of 150 W for 10 min. After cooling to 25 °C, the reaction was treated with water and the aqueous layer was extracted with

DCM (3 x 5 mL). The combined organic phases were washed with a saturated solution of NaCl, dried over anhydrous sodium sulphate, filtered and concentrated. Column chromatography on silica gel (2% MeOH in DCM) afforded the title compound as pale yellow oil (80% yield). ESI-MS *m/z*: 158 $[M\text{-H}]^-$.^{1}H NMR (300 MHz,$CDCl_3$) δ 7.27 (t, *J* = 9 Hz, 1H), 7.09 (t, *J* = 3 Hz, 2H), 7.00 – 6.97 (m, 1H), 6.89 (t, *J* = 3Hz, 1H), 6.74 – 6.71 (m, 1H), 6.38 (t, *J* = 3 Hz, 2H), 6.08 (br s, 1H). Spectroscopic data were consistent with previously reported ones.[46, 47]

1-(3-Hydroxyphenyl)-1*H*-pyrrole-2-carbonitrile (19). To a solution of compound **18** (50 mg, 0.31 mmol) in dry MeCN (5.0 mL) cooled to -20 °C, chlorosulfonyl isocyanate (67 mg, 0.47 mmol) was added and the mixture was stirred for 5 min at -20 °C and further 12 h at 25 °C. Then 1.0 ml of dry DMF was added and the mixture was heated to 55 °C and stirred for additional 20 min. Reaction was quenched with water and the aqueous layer was extracted with DCM (3 x 5 mL). The combined organic layers were washed with a saturated solution of NaCl, dried over anhydrous sodium sulphate, filtered and concentrated. Column chromatography on silica gel (20% EtOAc in petroleum ether) afforded the title compound as an amorphous white solid. (20% yield). ESI-MS *m/z*: 185 $[M\text{+H}]^+$. ^{1}H NMR (300 MHz, $CDCl_3$) δ 7.34 – 7.27 (m, 1H), 7.09 – 7.07 (m, 1H), 7.00 – 6.96 (m, 4H), 6.34 – 6.32 (m, 1H), 4.65 (br s, 1H).

1-(3-Hydroxyphenyl)-1*H*-pyrrole-2-carboxamide (20). Starting from **19** (70 mg, 0.38 mmol), the title compound was prepared according to the procedure followed for **7**. The crude was purified by means of silica gel column chromatography (30% petroleum ether in EtOAc) to afford **20** as a colourless oil (50% yield). ESI-MS *m/z*: 203 $[M\text{+H}]^+$. ^{1}H NMR (300 MHz, CD_3OD) δ 7.34 – 7.27 (m, 1H), 7.09 – 7.07 (m, 1H), 7.00 – 6.96 (m, 4H), 6.34 – 6.32 (m, 1H).

3-(2-Carbamoyl-1*H*-pyrrol-1-yl)phenyl (6-phenylhexyl)carbamate (3l). Starting from **20** (10 mg, 0.05 mmol) 6-phenylhexan-1-yl-isocyanate (40 mg, 0.20 mmol) and TEA (28 μL, 0.20

mmol), the title the title compound was prepared according to the procedure followed for **3h**. Silica gel column chromatography (1% MeOH in DCM) afforded **3l** an amorphous white solid (70% yield). ESI-MS *m/z*: 428 $[M+Na]^+$. ^1H NMR (300 MHz, CD_3OD) δ 7.39 (t, *J* = 6 Hz, 1H), 7.25 – 7.20 (m, 7H), 7.01 (t, *J* = 3Hz, 1H), 6.95 – 6.90 (m, 1H), 6.76 – 6.71 (m, 1H), 6.25 (m, 1H), 3.15 (t, *J* = 7.5 Hz, 2 H), 2.62 – 2.56 (m, 2H), 1.63 (m, 4H), 1.45 – 1.35 (m, 4H). ^{13}C NMR (75 MHz, CD_3OD) δ 164.6, 155.6, 151.6, 142.7, 141.6, 129.0, 128.4 128.2 (2C), 121.1 (2C), 126.4, 125.4, 122.2, 120.3, 118.9, 115.7, 108.9, 40.8, 35.6, 31.4, 29.5, 28.8, 26.5. Anal. ($C_{24}H_{27}N_3O_3$) C, H, N.

1-Bromo-9-methoxy-5,6-dihydro-4*H*-benzo[*f*]pyrrolo[1,2-*a*][1,4]diazepin-4-one (22). To a solution of **21** (821 mg, 3.6 mmol) in dry THF (20.0 mL) cooled at -70 °C, NBS (725 mg, 4.07 mmol) was added. The reaction mixture was stirred for 1,5 h at -70 °C and then gradually warmed to 25 °C and stirred for additional 12 h. Evaporation and column chromatography on silica gel (10% acetonitrile in DCM) and recrystallization from EtOAc afforded the title compound as a white crystalline solid. (45% yield). Mp = 190-193 °C. ESI-MS *m/z*: 307 $[M+H]^+$, 329 $[M+Na]^+$. ^1H NMR (400 MHz, $CDCl_3$) δ 7.50 (br s, 1H), 7.22 (d, *J* = 8.4 Hz, 1H), 7.07 (d, *J* = 2.4 Hz, 1H), 7.02 (d, *J* = 4.0 Hz, 1H), 6.83 (dd, *J* = 8.4, 2.5 Hz, 1H), 6.49 (d, *J* = 3.9 Hz, 1H), 4.31 (m, 1H), 3.89 (m, 1H), 3.81 (s, 3H).

9-Methoxy-4-oxo-5,6-dihydro-4*H*-benzo[*f*]pyrrolo[1,2-*a*][1,4]diazepine-1-carbonitrile (23). To a solution of **22** (496.0 mg, 1.61 mmol) in dry DMF (20.0 mL), CuCN (3,6 g, 25.00 mmol) was added. The reaction mixture was refluxed for 12 h, and then the crude was treated with a concentrated solution of NH_4OH and extracted with DCM. Evaporation and column chromatography on silica gel (10% acetonitrile in DCM) afforded the title compound as an amorphous white solid (30% yield). ESI-MS *m/z*: 254 $[M+H]^+$, 276 $[M+Na]^+$. ^1H NMR (300

MHz, $CDCl_3$) δ 7.38 (br s, 1H), 7.29 (s, 1H), 7.18 (d, *J* = 2.4 Hz, 1H), 7.08 - 7.03 (m, 2H), 6.92 (d, *J* = 8.4, 1H), 4.36 – 4.30 (m, 1H), 4.02 – 3.94 (m, 1H), 3.87 (s, 3H).

9-Hydroxy-4-oxo-5,6-dihydro-4*H*-benzo[*f*]pyrrolo[1,2-*a*][1,4]diazepine-1-carbonitrile (24). Starting from **23** (500 mg, 1.97 mmol), title compound was prepared according to the procedure followed for **12**. (30% yield). ESI-MS *m/z*: 238 $[M\text{-H}]^-$. ^{1}H NMR (400 MHz, acetone-d_6) δ 7.74 (br s, 1H), 7.31 (m, 1H), 7.19 (m, 2H), 6.87 (m, 2H), 4.25(m, 1H), 4.03 (m, 1H).

9-Hydroxy-4-oxo-5,6-dihydro-4*H*-benzo[*f*]pyrrolo[1,2-*a*][1,4]diazepine-1-carboxamide (25). Starting from **24** (45 mg, 0.19 mmol), title compound was prepared according to the procedure descripted for **7**. Purification on silica gel (DCM/MeOH/AcOH: 9,1,0.3) afforded **25** as yellow pale oil (40% yield). ESI-MS *m/z*: 256 $[M\text{-H}]^-$. ^{1}H NMR (400 MHz, MeOD) δ 7.20 (d, *J* = 8.3 Hz, 1H), 6.93 (d, *J* = 4.0 Hz, 1H), 6.89 (d, *J* = 4.0 Hz, 1H), 6.73 (dd, *J* = 8.2, 2.3 Hz, 1H), 6.61 (d, *J* = 2.3 Hz, 1H), 4.33 (d, *J* = 14.6 Hz, 1H), 3.95 (d, *J* = 14.6 Hz, 1H).

1-Carbamoyl-4-oxo-5,6-dihydro-4*H*-benzo[*f*]pyrrolo[1,2-*a*][1,4]diazepin-9-yl (6-phenylhexyl)carbamate (3m). Starting from **25** (50 mg, 0.19 mmol), the title the title compound was prepared according to the procedure followed for **3h**. Purification on silica gel (10% MeOH in DCM) afforded **3m** as an amorphous white solid (50% yield). ESI-MS *m/z*: 461 $[M\text{+H}]^+$. ^{1}H NMR (400 MHz, DMSO-d_6) δ 8.48 (br s, 1H), 7.87 (br s, 1H), 7.75 (t, *J* = 5.2 Hz, 1H), 7.39 (d, *J* = 8.2 Hz, 1H), 7.31 (br s, 1H), 7.22 (m, 2H), 7.15 -7.11 (m, 3H), 7.04 (d, *J* = 8.3 Hz, 1H), 6.84 (d, *J* = 3.8 Hz, 1H), 6.79 (d, *J* = 3.7 Hz, 1H), 6.74 (br s, 1H), 4.15 – 4.12 (m, 1H), 4.00 – 3.95 (m, 1H), 2.98 (m, 2H), 2.52 (m, 2H), 1.53 (m, 2H), 1.40 (m, 2H), 1.27 – 1.20 (m, 4H). ^{13}C NMR (75 MHz, DMSO-d_6) δ 162.7, 161.9, 154.0, 150.8, 142.8, 138.3, 134.0, 132.0, 130.2, 129.1, 129.0 (2C), 128.7, 126.3 (2C), 119.8, 119.0, 115.6, 115.5, 42.0, 35.7, 31.6, 29.7, 28.9, 28.1, 26.5. Anal. ($C_{26}H_{28}N_4O_4$) C, H, N.

X-Ray crystallography

A single crystal of compound **22** was submitted to X-ray data collection on an Oxford-Diffraction Xcalibur Sapphire 3 diffractometer with a graphite monochromated Mo-Kα radiation (λ = 0.71073 Å) at 293 K. The structure was solved by direct methods implemented in SHELXS program (Version 2013/1).[66] The refinement was carried out by full-matrix anisotropic least-squares on F2 for all reflections for non-H atoms by means of the SHELXL program.[67]

Crystallographic data have been deposited with the Cambridge Crystallographic Data Centre as supplementary publication no. CCDC 2008490.

Copies of the data can be obtained, free of charge, on application to CCDC, 12 Union Road, Cambridge CB2 1EZ, UK; (fax: + 44 (0) 1223 336 033; or e-mail: deposit@ccdc.cam.ac.uk).

Computational details

Ligands Preparation. Compounds were built by means of Maestro (Maestro, release 2018, Schrödinger LLC, New York, NY, 2018). Molecular energy minimizations were performed using MacroModel (MacroModel, release 2018, Schrödinger LLC, New York, NY, 2018) using OPLS3 as force field.[68] The solvent effects were simulated using the analytical Generalized-Born/Surface Area (GB/SA) model,[69] and no cutoff for nonbonded interactions was selected. Polak–Ribiere conjugate gradient (PRCG) method with 1000 maximum iterations and 0.001 gradient convergence threshold was used. All derivatives described in this work were treated by LigPrep application (LigPrep, release 2018, Schrödinger LLC, New York, NY, 2018), implemented in Maestro suite 2018, generating the most probable ionization state of any possible enantiomers and tautomers at cellular pH value (7.4 ± 0.5) and also for avoiding potential error in the structures.[41, 42,70-72]

Protein preparation. The three-dimensional structure of FAAH (PDB ID: 3PPM)[73] was taken from the PDB and imported into Schrödinger Maestro molecular modeling environment. Water molecules and compounds used for the crystallization were removed and the resulting structure was submitted to the protein preparation wizard implemented in Maestro suite 2018 as previously reported.[39, 40,74]

Molecular docking. Molecular docking was carried out using the Schrödinger suite 2018 employing the IFD protocol (Schrödinger Suite 2018 Induced Fit Docking protocol release 2018, Schrödinger LLC, New York, NY, 2012) as previously reported.[39, 40,75] Briefly, this procedure induces conformational changes in the binding site to accommodate the ligand and exhaustively identify possible binding modes and associated conformational changes by side-chain sampling and backbone minimization. The protein and the ligands used were prepared as reported in the previous paragraphs. The boxes for docking calculation were built taking into account the centroid of the co-crystallized ligand for the FAAH enzyme. Complexes within 30.0 kcal/mol of minimum energy structure were taken forward for redocking. The Glide redocking stage was performed by XP (Extra Precision) methods. The calculations were performed using default IFD protocol parameters. No hydrogen bonding or other constraints were used.

Molecular Properties Prediction. The *in silico* drug-like features of the designed compounds were evaluated by means of QikProp implemented in Maestro suite (QikProp, release 2018, Schrödinger, LLC, New York, NY, 2018).[76, 77]

Enzymatic assays

FAAH activity assay. Fatty acid amide hydrolase activity was assayed in homogenate mouse brain incubated at pH 9.0 with 10 μM [^{14}C]AEA (ARC, St. Louis, MO, USA) at 37 °C for 15 min (pH 9.0). The reaction was stopped with a 2:1 (v/v) mixture of chloroform/methanol, and the

release of [^{14}C]ethanolamine in the aqueous phase was measured as reported.[78] Control experiments were also carried out in the presence of the selective FAAH inhibitor URB597 (**1**). The effect of different compounds on FAAH activity was ascertained by adding each substance directly to the incubation medium.

MAGL activity assay. Mouse brain was thawed and homogenized at 4 °C in sodium phosphate buffer (50 mM, pH=8.0) containing 0.32 M sucrose. Homogenates were centrifuged at 4 °C sequentially at 800 g, 10,000 g, and 100,000g. MAGL activity was assayed in final supernatants at 100,000g, incubated with 10 μM [^{3}H] 2-OG (20 Ci/mmol; ARC, St. Louis, MO) at 37 °C for 30 min. The reaction was stopped with a 2:1 (v/v) mixture of chloroform/methanol and the release of [^{3}H]glycerol in the aqueous phase was measured by scintillation counting.[78]

Receptor binding assays

Mouse brain and spleen for CB1R and CB2R assay, respectively, was resuspended in 2 mM TrisEDTA, 320 mM sucrose, 5 mM $MgCl_2$ (pH 7.4), then it was homogenized in a Potter homogenizer and centrifuged three times at 1000g and the pellet was discharged. The supernatant was centrifuged at 18000g (30 min), and the pellet was resuspended in assay buffer (50 mM TrisHCl, 2mM TrisEDTA, 3 mM $MgCl_2$, pH 7.4). These membrane fractions were used in rapid filtration assays with radiolabel agonist [^{3}H]CP55,940 (PerkinElmer Life Sciences, Boston, MA, USA), as described previously.[78] In all experiments, nonspecific binding was determined in the presence of 1 μM "cold" agonist, and the effect of selective compounds for CB1R or CB2R was tested by adding each substance directly to the incubation medium.

Cytotoxicity and mutagenicity assays

Materials. Dulbecco's Modified Eagle's Medium, trypsin solution, and all the solvents used for cell culture were purchased from Lonza (Switzerland). Mouse immortalized fibroblasts

NIH3T3 and U-373-MG human glioblastoma astrocytoma were purchased from American Type Culture Collection (USA). The mutagenicity assay was supplied by Biologik s.r.l. (Trieste, Italy).

Cell cultures and cytotoxicity assay. NIH3T3 and U-373-MG were utilised for cytotoxicity experiments. Cells were maintained in DMEM at 37 °C in a humidified atmosphere containing 5% CO_2. The culture media were supplemented with 10% fetal calf serum (FCS), 1% *L*-glutamine-penicillin-streptomycin solution, and 1% MEM Non-Essential Amino Acid Solution. Once at the confluence, cells were washed with PBS 0.1 M, taken up with trypsin-EDTA solution and then centrifuged at 1000 rpm for 5 min. The pellet was re-suspended in medium solution (dilution 1:15). The stock solution for each compound was prepared in pure DMSO and diluted with complete culture medium. The solution/suspension obtained was then added to the cell monolayer. Cell viability after 24 h of incubation with the different concentrations of each test compound was evaluated by Neutral Red Uptake by the procedure previously reported.[79] The data processing included the Student's *t*-test with $p<0.05$ taken as the significance level.

First, the following solutions were prepared to determine the percentage of viable cells:

1. Neutral Red (NR) Stock Solution: 0.33 g NR Dye powder in 100 mL sterile H_2O

2. NR Medium: 1.0 mL NR Stock solution + 99.0 Routine Culture Medium pre-warmed to 37 °C

3. NR Desorb solution: 1% glacial acetic acid solution + 50% ethanol + 49% H_2O

At the end of the incubation, the routine culture medium was removed from each well, and cells were carefully rinsed with 1 mL of pre-warmed D-PBS. Multiwells were then gently blotted with paper towels. 1.0 mL of NR Medium was added to each well and further incubated at 37 °C, 95% humidity, 5.0% CO_2 for 3 h. The cells were checked during the NR incubation for NR crystal formation. After incubation, the NR Medium was removed; cells were carefully rinsed

with 1 mL of pre-warmed D-PBS. Then, the PBS was decanted and blotted from the wells and exactly 1 mL of NR Desorb solution was added to each sample. Multiwells were then put on a shaker for 20-45 min to extract NR from the cells and form a homogeneous solution. During this step, the samples were covered in order to protect them from light. After 5 min from the plate shaker removal, the absorbance was read at 540 nm by a UV/visible spectrophotometer (Lambda 25, Perkin Elmer).

Mutagenicity assay: Ames test. The TA100 and TA98 strains of *Salmonella Typhimurium* and S9 fraction were utilized for mutagenicity assay. Approximately 10^7 bacteria were exposed to 6 concentrations of each test compound, as well as a positive and negative control, for 90 min in a medium containing sufficient histidine to support approximately two cell divisions. After 90 min, the exposure cultures were diluted in a pH indicator medium lacking histidine and aliquoted into 48 wells of a 384-well plate. Within two days, cells that had undergone the reversion to *His* grew into colonies. Metabolism by the bacterial colonies reduced the pH of the medium, changing the colour of that well. This colour change can be detected visually or by a microplate reader. The number of wells containing reverting colonies were counted for each dose and compared to a zero dose control. Each dose was tested in six replicates. The test was performed both with and without S9 fraction.

Analysis of *in vitro* metabolic stability of 2a and 3h in human and liver microsomes

The tested compound (**2a** or **3h**), dissolved in MeCN, was incubated at 37 °C, at 5 μM concentration in 100 mM phosphate buffer (pH 7.4) with 0.3 mg/mL rat and human microsomal preparations as previously reported.[80] Enzymatic reactions were started by addition of a NADPH-regenerating system (2 mM NADPH), 66 mM glucose-6-phosphate, 0.4 U/mL glucose-6-phosphate dehydrogenase in 66 mM $MgCl_2$). Reactions were terminated at regular time

intervals (overall range 0-60 min) by adding a 1 mL of MeCN. All incubations were performed in triplicate. HPLC analysis was performed on Agilent 1100 Series liquid chromatography system equipped with an EC 150/4.6 nucleosil 100-3 C18 (Macherey-Nagel) and coupling with UV-VIS detector, setting at λ 254 nm. The analysis was carried out using gradient elution of a binary solution; eluent A was MeCN (MeCN containing 0.1% formic acid), while eluent B consisting of an aqueous solution of formic acid (0.1%). The analysis started at 20% A for three minutes, then rapidly increased up to 90% in 15 min and finally remaining at 90% A until 25 min. The analysis was performed at a flow rate of 0.8 mL min^{-1} and injection volume was 20 µL. The intrinsic clearance (Clint) was calculated by the equation:

Clint = k(min-1)x [V]/[P]

where k is the rate constant for the depletion of the substrate, V is the volume of incubation in µL and P is the amount of microsomal proteins as reported elsewhere.[81]

Oxidative stress

Cell culture and treatments. IMR32 cells (obtained from American Type Culture Collection, ATCC) were cultured as described in our previous work.[42] Stock solutions of compounds **3h**, **3m**, and **2a** were prepared in DMSO and diluted just prior use into the cell culture medium to reach the final concentrations of the assays (0.1 µM, 0.5 µM, 1 µM, 5 µM, 10 µM and 50 µM). Control vehicle was represented by DMSO ranging from 0.5% to 0.001%. Lipopolysaccharide (LPS) from Escherichia coli serotype 0111:B4 was purchased from Sigma-Aldrich (Sigma-Aldrich Corp., St. Louis, MO, USA). LPS was dissolved in phosphate-buffered saline (PBS) solution.

Cytotoxicity determination. Cytotoxic effects of the different compounds on IMR32 cells were evaluated by measurement of LDH (lactate dehydrogenase) release into the cell culture medium.

Briefly, IMR32 cells were seeded into a 96-well plate at 100,000 cells/well and allowed to grow at the confluence. Then, cells were treated with compounds **3h**, **3m**, and **2a** at different concentrations (0.1 μM, 0.5 μM, 1 μM, 5 μM, 10 μM and 50 μM). After 24 hours of incubation, LDH assay was performed according to the manufacturer's protocol (Euroclone, Milan, Italy). All tests were performed at least in triplicate. The absorbance measured from three wells was averaged and the percentage of LDH release was calculated as an arbitrary unit of change relative to 2% (v/v) Triton X-100 treated cells.

Nuclear proteins extraction. IMR32 cells were seeded in 100 mm Petri dishes and allowed to grow at the confluence. After treatment with compounds **3h**, **3m**, and **2a** at 0.5 and 1 μM doses for 24 h, cells were challenged with 100 μg/ml LPS for 30 minutes. Then, cells were detached, washed with ice-cold PBS 1X and pelleted by centrifugation. Cell pellets were processed as previously described.[82] The supernatant containing the cytosolic proteins was removed and the pellet containing the nuclei was suspended in the nuclear extraction buffer containing: 20 mmol/L HEPES (pH 7.9), 0,6 mol/L KCl, 1.5 mmol/L $MgCl_2$, 20% glycerol, 0.5 mmol/L phenyl-methyl-sulphonyl fluoride and protease and phosphatase inhibitor cocktails. After 30 minutes of incubation on ice with intermitted mixing, samples were centrifuged at 21,100 x g for 15 minutes to obtain the nuclear protein fractions. Protein concentration was determined using a Bradford protein assay (Bio-Rad Protein Assay; Bio-Rad Laboratories, Inc, Milan, Italy).

NF-κB p65 DNA binding activity in nuclear extracts. The DNA-binding activity of NF-kB p65 subunit in IMR32 cell nuclear extracts was quantified using the TransAM NF-kB p65 Transcription Factor Assay Kit (Active Motif North America, Carlsbad, CA, USA). Briefly, five micrograms of nuclear protein extracts were incubated with NF-κB p65 consensus binding sites (5′-GGG ACT TTCC-3′) immobilized on a 96-well plate for 1 h at rt. Then, a secondary

antibody conjugated with a horseradish peroxidase provides a colorimetric output, spectrophotometrically detected at 450 nm. NF-κB p65 binding to the oligonucleotides was detected by incubation with a primary antibody specific for the activated form of p65 (Active Motif North America), HRP-conjugated secondary antibody and developing solution. The absorbance at 450 nm was determined with a microplate reader. Results were normalized for nuclear extract protein concentrations.

Statistical analysis. All the results are expressed as mean ± SD of triplicate determinations obtained in three independent experiments. For each of the variables tested, a two-way analysis of variance (ANOVA) was used. P values < 0.05 were considered statistically significant. Data were analyzed using the software GraphPad Prism 4.0 (GraphPad Software, Inc., La Jolla, CA).

Langendorff perfused rat heart

Animals. All animal care and experimental protocols conformed to the European Union Guidelines for the Care and the Use of Laboratory Animals (European Union Directive 2010/63/EU) and were approved by the Italian Department of Health (666/2015-PR). Male Wistar rats (300-350 g, Charles River Italia, Calco, Italy) were anesthetized (i.p.) with a mixture of Zoletil® 100 (7.5 mg/kg tiletamine HCl + 7.5 mg/kg zolazepam HCl; Virbac srl, Milano) e Rompun® (8 mg/kg xylazine HCl; Bio 98, San Lazzaro, Bologna), containing heparin (5000 U/kg), decapitated and exsanguinated.

Isolated Rat Heart Preparation and Perfusion. The hearts, spontaneously beating, were rapidly explanted and mounted on a Langendorff apparatus for retrograde perfusion via the aorta at a constant flow rate of 10 mL/min with a Krebs−Henseleit solution of the following composition (mM): NaCl 118, KCl 4.7, $CaCl_2$ 2.5, $MgSO_4$ 1.2, $NaHCO_3$ 25, KH_2PO_4 1.2, glucose 11.5, Na pyruvate 2, and EDTA 0.5, bubbled with a 95% O_2−5% CO_2 gas mixture (pH

7.4), and kept at 37 °C, as described elsewhere.[83] Hearts were allowed to equilibrate for at least 20 min before drug exposure.

Heart contractility was measured as left ventricle pressure (LVP) by means of latex balloon, inserted into the left ventricle via the mitral valve and connected to a pressure transducer (BLPR, WPI, Berlin, Germany). The balloon was inflated with deionized water from a microsyringe until a left ventricular end-diastolic pressure of 10 mmHg was obtained. Alteration in coronary perfusion pressure (CPP), arising from changes in coronary vascular resistance, was recorded by a pressure transducer (BLPR, WPI, Berlin, Germany) placed in the inflow line.[84]

A surface electrocardiogram (ECG) was recorded at a sampling rate of 1 kHz by means of two steel electrodes, one placed on the apex and the other on the left atrium of the heart. The ECG analysis included the following measurements: RR (cycle length), HR (frequency), PQ (atrioventricular conduction time), QRS (intraventricular conduction time), and QT (overall action potential duration).[85]

LVP, CPP, and ECG were recorded with a digital PowerLab data acquisition system (PowerLab 8/30; ADInstruments, Castle Hill, Australia) and analyzed by using Chart Pro for Windows software (PowerLab; ADInstruments, Castle Hill, Australia). LVP was calculated by subtracting the left ventricular diastolic pressure from the left ventricular systolic pressure. As the QT interval is affected by heart rate changes (e.g., it shortens when the heart rate increases), Bazett's formula normalized to average rat RR ($QTc=QT/(RR/f)1/2$)[86] was routinely used to correct it, in order to avoid confounding effects. In our experiments, “f”, the normalization factor according to the basal RR duration was 232.18 ms, as it was the average cardiac cycle length. Analysis of data was accomplished using GraphPad Prism version 5.04 (GraphPad Software, San Diego, USA). Statistical analyses and significance as measured by repeated measures ANOVA

(followed by Dunnett's post-test) were obtained using GraphPad InStat version 3.06 (GraphPad Software, San Diego, USA). In all comparisons, $P < 0.05$ was considered significant.

Compound **3h** was dissolved in DMSO. Solvent failed to alter the response of the preparations (data not shown).

***In vivo* studies on animal models of epilepsy**

Animals. Adult male Sprague–Dawley rats (225–250 g) were housed at constant temperature (23 °C) and relative humidity (60%), with free access to food and water and a fixed 12-hour light/dark cycle. All animal use followed the University of Pittsburgh and University of Malta Institutional Animal Care and Use guidelines and was in strict accordance with the National Institutes of Health Guide for the Care and Use of Laboratory Animals, USA and the EU Directive 2010/63/EU for animal experiments, respectively.

Drugs. Compound **2a** and **3h** were freshly dissolved in a vehicle (2 mL/kg) of 5% PEG-400, 5% Tween 80 in saline and administered intraperitoneally (i.p.). Pilocarpine, scopolamine methyl-hydrate and other common salts were bought from SIGMA.

Maximal dentate activation (MDA). Surgical procedure and electrode implantation. Urethane anaesthetized rats (1.2 g/kg, i.p.) were positioned in a David Kopf stereotaxic frame and their body temperature maintained using a heating pad and temperature controller unit (Temperature Control Unit HB 101/2, Letica Scientific Instruments). One electrode (bifilar stainless steel wire, CFW, CA, USA) was implanted in the entorhinal cortex to stimulate the perforant pathway (PP; AP: -7.9 L: 4.6 V: 3.4) and another in the hilus of the dentate gyrus (DG) of the hippocampus (AP: -4.8 L: 2.5 V: 3.6) to record field potentials. During the surgery, electrodes were slowly lowered until the optimal depth to record population spikes (PSs) was reached. Field potentials were recorded by a NeuroLog amplifier (Digitimer Ltd, high pass: 0.2 Hz, low pass: 5,000 Hz,

gain: 200). A digitally controlled current stimulator (Digitimer Ltd, model DS3) was used to apply square-wave pulses of 0.2 ms at a rate of 1 per minute. Stimulus intensity was set to evoke 40-50% of the maximum amplitude of the PSs. Responses were digitized by a CED 1401 plus analogue–digital converter (Cambridge Electronic Design Ltd., Cambridge, UK), stored on a computer and averaged offline using Signal 1.9 software. The sampling rate was set to 10 kHz. The location of the electrodes was verified histologically.

MDA induction. To initiate MDA, stimulus trains (pulses of 0.3 ms duration, at 20 Hz) of 10s were delivered to the PP at 200 μA initially. If MDA could not be induced, the stimulus intensity was increased by 50 μA and redelivered and the process repeated every 5 mins until MDA was induced. Stimulus-trains were given every 10 min for 4h (total of 24 stimulus trains) and for each train, the duration and time to onset of MDA were measured. Measurements of MDA are shown in Figure S4. The time to onset indicates the time (in a sec) from the beginning of the stimulus train to the point where PSs appeared with half of the maximal amplitude. The duration of the MDA was measured from the onset to the end of the after discharges (ADs). ADs are represented by spontaneous bursts of PSs that appear after the stimulus train. Duration and time to onset of MDA were normalized against the first stimulus train to give the value of a change in duration or time to onset so that data from separate animals could be averaged and compared. **2a** was injected after stimulus train 6.

Long-term potentiation (LTP). Tetanic high-frequency stimulation (HFS) consisting of 10 trains of 15 pulses of 200 Hz with a 1s delay between trains was used to induce long-term potentiation (LTP, 200 Hz) at PP-DG synapses. The effect of **2a** on LTP was tested in a first set of experiments where HFS was delivered 30 min after **2a** administration. 10 min baseline recordings were taken prior to drug treatment and LTP was recorded for 120 mins after the HFS.

Pulse strength was set to evoke 40-50% of the maximum PS amplitude and remained unchanged for all stimulations. For baseline and post-HFS recordings, single pulses were applied every 60s, and 5 responses were averaged.

Pilocarpine Model of Status Epilepticus. Sprague Dawley rats (225–250 g) were treated with vehicle, **2a** or **3h** (2, 5 or 10 mg/kg, i.p.) then after 15 mins injected with scopolamine methyl-hydrate (1 mg/kg in saline, i.p.) to prevent any peripheral cholinergic side effects and after 45 min pilocarpine was administered (360 mg/kg in saline, i.p.). Rats were then recorded for 2 h from the onset of status epilepticus (SE) and seizures scored from 0 to 5 on the Racine scale. The duration of the seizure and the time to onset of SE were also recorded. 2 h after the first seizure induced by PILO injection diazepam (10 mg/kg, i.p.) was administered and SE remitted.

Histological Labelling of Thiols. The assay was performed accordingly with Horowitz et al.[87] Briefly, animals were sacrificed by decapitation 24 h after diazepam treatment to block pilocarpine-induced SE, their brains were removed and frozen in liquid nitrogen and stored for 24 h at -80 °C to allow them to freeze homogeneously. For redox staining, frozen brains were placed in the first alkylating solution (4% paraformaldehyde, 10 μM NEM, 1 μM Alexa-NEM 680 nm, Triton X-100 0.02% in PBS) and protected from direct light and stored for 5 days at 4 °C. The solution was then replaced with 30% sucrose solution until brains sank. Brains were then frozen in dry ice, cut on a microtome and the slices placed in a multi-well plate containing PBS. Slices were then washed with PBS 3 times for 5 min each time. Before being exposed to a reducing solution (50 mM TCEP in PBS) and incubated for 30 min at room temperature out of direct light. Slices were then exposed to a second alkylating solution (10 μM *N*-ethylmaleimide, 1μM Alexa-*N*-ethylmaleimide 540 nm, Triton X-100 0.02% in PBS) before washing with PBS (3 x 5 min) and mounted on slides. An Olympus Fluoview 1000 laser scanning confocal

microscope was used for the ratiometric confocal analysis of thiols and disulphides. A 1 μm thick optical slice was taken with a manually generated region-of-interest (ROI). Signal intensity and the ratio S-S/S-H signal were measured by the software and parameters were set in the control reaction and kept constant. Ratios were taken against control animals treated with vehicle only.

Statistical analysis. Statistical analysis was performed using statistical software package GraphPad Prism4 (San Diego, CA). The data were expressed as means ± SEM. Statistical significance was determined at the level of $p \leq 0.05$. The data obtained were compared by the One-way ANOVA analysis of variance followed by Bonferroni post-hoc multiple comparisons or Turkey's Multiple Comparison tests.

ASSOCIATED CONTENT

Supporting Information Available: The Supporting Information including Figures S1-S4 Table S1 and Table S2 (Elemental analysis for compounds **3a-m**) is available free of charge on the ACS Publications website at xxxxxxx.

AUTHOR INFORMATION

Alessandro Grillo, 0000-0003-4472-4978

Filomena Fezza, 0000-0003-2263-2909

Giulia Chemi, 0000-0002-3868-6752

Roberto Colangeli, 0000-0002-3441-0492

Simone Brogi, 0000-0001-9375-6242

Domenico Fazio, 0000-0002-1235-9999

Stefano Federico, 0000-0002-7478-6128

Alessandro Papa, 0000-0001-8141-3648

Nicola Relitti, 0000-0001-9783-8966

Roberto Di Maio, 0000-0003-2162-1781

Gianluca Giorgi, 0000-0002-8817-7745

Stefania Lamponi, 0000-0002-2788-8797

Massimo Valoti, 0000-0002-7240-3576

Beatrice Gorelli, 0000-0003-4909-5103

Simona Saponara, 0000-0002-3831-8669

Mascia Benedusi, 0000-0002-4656-8609

Alessandra Pecorelli, 0000-0002-5207-068X

Giuseppe Valacchi, 0000-0002-8792-0947

Stefania Butini, 0000-0002-8471-0880

Giuseppe Campiani, 0000-0001-5295-9529

Sandra Gemma, 0000-0002-8313-2417

Mauro Maccarrone, 0000-0002-3990-2963

Giuseppe Di Giovanni, 0000-0003-2006-563X

Corresponding Author

*To whom correspondence should be addressed, Stefania Butini email: butini3@unisi.it; Giuseppe Campiani email: campiani@unisi.it.

Present Addresses

[†]Alessandro Grillo present address: Promidis S.r.L. Via Olgettina 60, Milano, Torre San Michele 1, ospedale San Raffaele

†Giulia Chemi present address: Wellcome Centre for Anti-Infectives Research, Drug Discovery Unit, Division of Biological Chemistry and Drug Discovery, University of Dundee, Dundee DD1 5EH, UK

†Nicola Relitti present address: IRBM Science Park, Via Pontina km 30,600, 00071 Pomezia, Rome, Italy

†Patrizia Minetti present address: Via Giorgio Vigolo, 40, 00143 Roma, Italy

Author Contributions

The manuscript was written through the contributions of all authors. All authors approved the final version of the manuscript.

°Equally senior authors.

ABBREVIATIONS

2-AG, 2-arachidonoyl-glycerol; ADs, after discharges; AEA, anandamide; CB1R, cannabinoid receptor type 1; CB2R, cannabinoid receptor type 2; CPP, coronary perfusion pressure; DCM, dichloromethane; DG, dentate gyrus; DMAP, 4-(dimethylamino)pyridine; DMF, dimethylformamide; DMSO, dimethyl sulfoxide; DSE, depolarization-induced suppression of excitation; DSI, depolarization-induced suppression of inhibition; ECG, electrocardiogram; ECS, endocannabinoid system; FAAH, fatty acid amide hydrolase; FCS, fetal calf serum; GB/SA, Generalized Born/Surface Area; HFS, high-frequency stimulation; HLM, human liver microsomes; HR, frequency; IFD, Induced Fit Docking; ILAE, International League Against Epilepsy; LDH, lactate dehydrogenase; LTP, Long term potentiation; LVP, left ventricle

pressure; MAGL, monoacylglycerol lipase; MDA, Maximal Dentate Activation; MW, microwave; NBS, *N*-bromosuccinimmide; NRU, Neutral Red Uptake; OS, oxidative stress; PP, perforant path; PQ, atrioventricular conduction time; PRCG, Polak-Ribiere conjugate gradient; PS, population spike; QRS, intraventricular, conduction time; QT, overall action potential duration; RLM, rat liver microsomes; ROI, region-of-interest; RR, cycle length; SAR, structure-activity relationship; SE, status epilepticus; STP-LTP, short-term and long term plasticity; TEA, triethylamine; THF, tetrahydrofuran; TLC, thin layer chromatography; TLE, temporal lobe epilepsy; XP, Extra Precision.

ACKNOWLEDGMENT

This work was supported by Malta Council of Science and Technology, grant R&I-2013-14 EPILEFREE to GDG. RC was supported by a fellowship funded by EPILEFREE. The authors wish to thank MIUR-PRIN n° 20175SA5JJ for financial support.

References

1. Pacher, P.; Kunos, G., Modulating the endocannabinoid system in human health and disease--successes and failures. *Febs J* **2013,** *280* (9), 1918-1943.
2. Romigi, A.; Bari, M.; Placidi, F.; Marciani, M. G.; Malaponti, M.; Torelli, F.; Izzi, F.; Prosperetti, C.; Zannino, S.; Corte, F.; et al., Cerebrospinal fluid levels of the endocannabinoid anandamide are reduced in patients with untreated newly diagnosed temporal lobe epilepsy. *Epilepsia* **2010,** *51* (5), 768-772.
3. Di Maio, R.; Mastroberardino, P. G.; Hu, X.; Montero, L. M.; Greenamyre, J. T., Thiol oxidation and altered NR2B/NMDA receptor functions in in vitro and in vivo pilocarpine models: implications for epileptogenesis. *Neurobiology of disease* **2013,** *49*, 87-98.
4. Cope, D. W.; Di Giovanni, G.; Fyson, S. J.; Orban, G.; Errington, A. C.; Lorincz, M. L.; Gould, T. M.; Carter, D. A.; Crunelli, V., Enhanced tonic GABAA inhibition in typical absence epilepsy. *Nat Med* **2009,** *15* (12), 1392-1398.
5. Toczek, M.; Malinowska, B., Enhanced endocannabinoid tone as a potential target of pharmacotherapy. *Life sciences* **2018,** *204*, 20-45.
6. Saario, S. M.; Laitinen, J. T., Therapeutic potential of endocannabinoid-hydrolysing enzyme inhibitors. *Basic & clinical pharmacology & toxicology* **2007,** *101* (5), 287-293.

7. Fisher, R. S.; Acevedo, C.; Arzimanoglou, A.; Bogacz, A.; Cross, J. H.; Elger, C. E.; Engel, J., Jr.; Forsgren, L.; French, J. A.; Glynn, M.; et al., ILAE official report: a practical clinical definition of epilepsy. *Epilepsia* **2014,** *55* (4), 475-482.
8. Bell, G. S.; Sander, J. W., The epidemiology of epilepsy: the size of the problem. *Seizure* **2001,** *10* (4), 306-314; quiz 315-316.
9. Kotsopoulos, I. A.; van Merode, T.; Kessels, F. G.; de Krom, M. C.; Knottnerus, J. A., Systematic review and meta-analysis of incidence studies of epilepsy and unprovoked seizures. *Epilepsia* **2002,** *43* (11), 1402-1409.
10. Carpio, A.; Hauser, W. A., Epilepsy in the developing world. *Current neurology and neuroscience reports* **2009,** *9* (4), 319-326.
11. Wass, C. T.; Rajala, M. M.; Hughes, J. M.; Sharbrough, F. W.; Offord, K. P.; Rademacher, D. M.; Lanier, W. L., Long-term follow-up of patients treated surgically for medically intractable epilepsy: results in 291 patients treated at Mayo Clinic Rochester between July 1972 and March 1985. *Mayo Clinic proceedings* **1996,** *71* (11), 1105-1113.
12. Keene, D. L.; Higgins, M. J.; Ventureyra, E. C., Outcome and life prospects after surgical management of medically intractable epilepsy in patients under 18 years of age. *Child's nervous system : ChNS : official journal of the International Society for Pediatric Neurosurgery* **1997,** *13* (10), 530-535.
13. Semah, F.; Picot, M. C.; Adam, C.; Broglin, D.; Arzimanoglou, A.; Bazin, B.; Cavalcanti, D.; Baulac, M., Is the underlying cause of epilepsy a major prognostic factor for recurrence? *Neurology* **1998,** *51* (5), 1256-1262.
14. Kanner, A. M., Depression in epilepsy: prevalence, clinical semiology, pathogenic mechanisms, and treatment. *Biological psychiatry* **2003,** *54* (3), 388-398.
15. Kotloski, R.; Lynch, M.; Lauersdorf, S.; Sutula, T., Repeated brief seizures induce progressive hippocampal neuron loss and memory deficits. *Progress in brain research* **2002,** *135*, 95-110.
16. Ferriero, D. M., Protecting neurons. *Epilepsia* **2005,** *46 Suppl 7*, 45-51.
17. Valacchi, G.; Virgili, F.; Cervellati, C.; Pecorelli, A., OxInflammation: From Subclinical Condition to Pathological Biomarker. *Frontiers in physiology* **2018,** *9*, 858.
18. Shin, E. J.; Jeong, J. H.; Chung, Y. H.; Kim, W. K.; Ko, K. H.; Bach, J. H.; Hong, J. S.; Yoneda, Y.; Kim, H. C., Role of oxidative stress in epileptic seizures. *Neurochem Int* **2011,** *59* (2), 122-137.
19. Pecorelli, A.; Natrella, F.; Belmonte, G.; Miracco, C.; Cervellati, F.; Ciccoli, L.; Mariottini, A.; Rocchi, R.; Vatti, G.; Bua, A.; et al., NADPH oxidase activation and 4-hydroxy-2-nonenal/aquaporin-4 adducts as possible new players in oxidative neuronal damage presents in drug-resistant epilepsy. *Biochimica et biophysica acta* **2015,** *1852* (3), 507-519.
20. Asadi-Pooya, A. A.; Stewart, G. R.; Abrams, D. J.; Sharan, A., Prevalence and Incidence of Drug-Resistant Mesial Temporal Lobe Epilepsy in the United States. *World neurosurgery* **2017,** *99*, 662-666.
21. Wilson, R. I.; Nicoll, R. A., Endogenous cannabinoids mediate retrograde signalling at hippocampal synapses. *Nature* **2001,** *410* (6828), 588-592.
22. Alger, B. E., Endocannabinoids and their implications for epilepsy. *Epilepsy currents* **2004,** *4* (5), 169-173.
23. van Rijn, C. M.; Gaetani, S.; Santolini, I.; Badura, A.; Gabova, A.; Fu, J.; Watanabe, M.; Cuomo, V.; van Luijtelaar, G.; Nicoletti, F.; et al., WAG/Rij rats show a reduced expression of

CB(1) receptors in thalamic nuclei and respond to the CB(1) receptor agonist, R(+)WIN55,212-2, with a reduced incidence of spike-wave discharges. *Epilepsia* **2010,** *51* (8), 1511-1521.
24. Magloczky, Z.; Toth, K.; Karlocai, R.; Nagy, S.; Eross, L.; Czirjak, S.; Vajda, J.; Rasonyi, G.; Kelemen, A.; Juhos, V.; et al., Dynamic changes of CB1-receptor expression in hippocampi of epileptic mice and humans. *Epilepsia* **2010,** *51 Suppl 3*, 115-120.
25. Treiman, D. M., GABAergic mechanisms in epilepsy. *Epilepsia* **2001,** *42 Suppl 3*, 8-12.
26. Maccarrone, M.; Guzman, M.; Mackie, K.; Doherty, P.; Harkany, T., Programming of neural cells by (endo)cannabinoids: from physiological rules to emerging therapies. *Nat Rev Neurosci* **2014,** *15* (12), 786-801.
27. Lastres-Becker, I.; Hansen, H. H.; Berrendero, F.; De Miguel, R.; Perez-Rosado, A.; Manzanares, J.; Ramos, J. A.; Fernandez-Ruiz, J., Alleviation of motor hyperactivity and neurochemical deficits by endocannabinoid uptake inhibition in a rat model of Huntington's disease. *Synapse* **2002,** *44* (1), 23-35.
28. Ramirez, B. G.; Blazquez, C.; Gomez del Pulgar, T.; Guzman, M.; de Ceballos, M. L., Prevention of Alzheimer's disease pathology by cannabinoids: neuroprotection mediated by blockade of microglial activation. *The Journal of neuroscience : the official journal of the Society for Neuroscience* **2005,** *25* (8), 1904-1913.
29. Marsicano, G.; Goodenough, S.; Monory, K.; Hermann, H.; Eder, M.; Cannich, A.; Azad, S. C.; Cascio, M. G.; Gutierrez, S. O.; van der Stelt, M.; et al., CB1 cannabinoid receptors and on-demand defense against excitotoxicity. *Science* **2003,** *302* (5642), 84-88.
30. Wallace, M. J.; Blair, R. E.; Falenski, K. W.; Martin, B. R.; DeLorenzo, R. J., The endogenous cannabinoid system regulates seizure frequency and duration in a model of temporal lobe epilepsy. *J Pharmacol Exp Ther* **2003,** *307* (1), 129-137.
31. Auclair, N.; Otani, S.; Soubrie, P.; Crepel, F., Cannabinoids modulate synaptic strength and plasticity at glutamatergic synapses of rat prefrontal cortex pyramidal neurons. *Journal of neurophysiology* **2000,** *83* (6), 3287-3293.
32. Abush, H.; Akirav, I., Short- and long-term cognitive effects of chronic cannabinoids administration in late-adolescence rats. *PloS one* **2012,** *7* (2), e31731.
33. Mechoulam, R.; Parker, L. A., The endocannabinoid system and the brain. *Annual review of psychology* **2013,** *64*, 21-47.
34. Blair, R. E.; Deshpande, L. S.; Sombati, S.; Elphick, M. R.; Martin, B. R.; DeLorenzo, R. J., Prolonged exposure to WIN55,212-2 causes downregulation of the CB1 receptor and the development of tolerance to its anticonvulsant effects in the hippocampal neuronal culture model of acquired epilepsy. *Neuropharmacology* **2009,** *57* (3), 208-218.
35. Vilela, L. R.; Medeiros, D. C.; Rezende, G. H.; de Oliveira, A. C.; Moraes, M. F.; Moreira, F. A., Effects of cannabinoids and endocannabinoid hydrolysis inhibition on pentylenetetrazole-induced seizure and electroencephalographic activity in rats. *Epilepsy research* **2013,** *104* (3), 195-202.
36. Karanian, D. A.; Karim, S. L.; Wood, J. T.; Williams, J. S.; Lin, S.; Makriyannis, A.; Bahr, B. A., Endocannabinoid enhancement protects against kainic acid-induced seizures and associated brain damage. *J Pharmacol Exp Ther* **2007,** *322* (3), 1059-1066.
37. Panlilio, L. V.; Thorndike, E. B.; Nikas, S. P.; Alapafuja, S. O.; Bandiera, T.; Cravatt, B. F.; Makriyannis, A.; Piomelli, D.; Goldberg, S. R.; Justinova, Z., Effects of fatty acid amide hydrolase (FAAH) inhibitors on working memory in rats. *Psychopharmacology* **2016,** *233* (10), 1879-1888.

38. Colangeli, R.; Pierucci, M.; Benigno, A.; Campiani, G.; Butini, S.; Di Giovanni, G., Author Correction: The FAAH inhibitor URB597 suppresses hippocampal maximal dentate afterdischarges and restores seizure-induced impairment of short and long-term synaptic plasticity. *Scientific reports* **2018,** *8* (1), 17977.
39. Butini, S.; Brindisi, M.; Gemma, S.; Minetti, P.; Cabri, W.; Gallo, G.; Vincenti, S.; Talamonti, E.; Borsini, F.; Caprioli, A.; et al., Discovery of potent inhibitors of human and mouse fatty acid amide hydrolases. *J Med Chem* **2012,** *55* (15), 6898-6915.
40. Butini, S.; Gemma, S.; Brindisi, M.; Maramai, S.; Minetti, P.; Celona, D.; Napolitano, R.; Borsini, F.; Cabri, W.; Fezza, F.; et al., Identification of a novel arylpiperazine scaffold for fatty acid amide hydrolase inhibition with improved drug disposition properties. *Bioorg Med Chem Lett* **2013,** *23* (2), 492-495.
41. Brindisi, M.; Borrelli, G.; Brogi, S.; Grillo, A.; Maramai, S.; Paolino, M.; Benedusi, M.; Pecorelli, A.; Valacchi, G.; Di Cesare Mannelli, L.; et al., Development of Potent Inhibitors of Fatty Acid Amide Hydrolase Useful for the Treatment of Neuropathic Pain. *ChemMedChem* **2018,** *13* (19), 2090-2103.
42. Grillo, A.; Chemi, G.; Brogi, S.; Brindisi, M.; Relitti, N.; Fezza, F.; Fazio, D.; Castelletti, L.; Perdona, E.; Wong, A.; et al., Development of novel multipotent compounds modulating endocannabinoid and dopaminergic systems. *Eur J Med Chem* **2019,** *183*, 111674.
43. Brindisi, M.; Brogi, S.; Maramai, S.; Grillo, A.; Borrelli, G.; Butini, S.; Novellino, E.; Allara, M.; Ligresti, A.; Campiani, G.; et al., Harnessing the pyrroloquinoxaline scaffold for FAAH and MAGL interaction: definition of the structural determinants for enzyme inhibition. *Rsc Adv* **2016,** *6* (69), 64651-64664.
44. Gemma, S.; Colombo, L.; Forloni, G.; Savini, L.; Fracasso, C.; Caccia, S.; Salmona, M.; Brindisi, M.; Joshi, B. P.; Tripaldi, P.; et al., Pyrroloquinoxaline hydrazones as fluorescent probes for amyloid fibrils. *Org Biomol Chem* **2011,** *9* (14), 5137-5148.
45. Contreras, J. M.; Parrot, I.; Sippl, W.; Rival, Y. M.; Wermuth, C. G., Design, synthesis, and structure-activity relationships of a series of 3-[2-(1-benzylpiperidin-4-yl)ethylamino]pyridazine derivatives as acetylcholinesterase inhibitors. *J Med Chem* **2001,** *44* (17), 2707-2718.
46. Maria Chatzopoulou; Eleni Kotsampasakou; Demopoulos, V. J., Clauson–Kaas-type synthesis of pyrrolylphenols, from the hydrochlorides of aminophenols, in the presence of nicotinamide. *Synthetic Commun* **2013,** *43*, 6.
47. Oliver, J. E.; Lusby, W. R.; Waters, R. M., Rearrangements of Pyrrole and Indole Substituted Enol Esters of Cyclohexane-1,3-Dione. *J Heterocyclic Chem* **1991,** *28* (6), 1565-1568.
48. Moreno-Sanz, G.; Duranti, A.; Melzig, L.; Fiorelli, C.; Ruda, G. F.; Colombano, G.; Mestichelli, P.; Sanchini, S.; Tontini, A.; Mor, M.; et al., Synthesis and Structure-Activity Relationship Studies of O-Biphenyl-3-yl Carbamates as Peripherally Restricted Fatty Acid Amide Hydrolase Inhibitors. *J Med Chem* **2013,** 56 (14), 5917-5930.
49. Johnson, D. S.; Weerapana, E.; Cravatt, B. F., Strategies for discovering and derisking covalent, irreversible enzyme inhibitors. *Future medicinal chemistry* **2010,** *2* (6), 949-64.
50. Brindisi, M.; Butini, S.; Franceschini, S.; Brogi, S.; Trotta, F.; Ros, S.; Cagnotto, A.; Salmona, M.; Casagni, A.; Andreassi, M.; et al., Targeting dopamine D3 and serotonin 5-HT1A and 5-HT2A receptors for developing effective antipsychotics: synthesis, biological characterization, and behavioral studies. *J Med Chem* **2014,** *57* (22), 9578-9597.

51. Orban, G.; Pierucci, M.; Benigno, A.; Pessia, M.; Galati, S.; Valentino, M.; Muscat, R.; Di Giovanni, G., High dose of 8-OH-DPAT decreases maximal dentate gyrus activation and facilitates granular cell plasticity in vivo. *Exp Brain Res* **2013,** *230* (4), 441-451.
52. Stringer, J. L.; Lothman, E. W., Maximal dentate activation: a tool to screen compounds for activity against limbic seizures. *Epilepsy research* **1990,** *5* (3), 169-176.
53. Orban, G.; Bombardi, C.; Marino Gammazza, A.; Colangeli, R.; Pierucci, M.; Pomara, C.; Pessia, M.; Bucchieri, F.; Benigno, A.; Smolders, I.; et al., Role(s) of the 5-HT2C receptor in the development of maximal dentate activation in the hippocampus of anesthetized rats. *CNS Neurosci Ther* **2014,** *20* (7), 651-661.
54. Colangeli, R.; Pierucci, M.; Benigno, A.; Campiani, G.; Butini, S.; Di Giovanni, G., The FAAH inhibitor URB597 suppresses hippocampal maximal dentate afterdischarges and restores seizure-induced impairment of short and long-term synaptic plasticity. *Sci Rep* **2017,** *7* (1), 11152.
55. Terranova, J. P.; Michaud, J. C.; Le Fur, G.; Soubrie, P., Inhibition of long-term potentiation in rat hippocampal slices by anandamide and WIN55212-2: reversal by SR141716 A, a selective antagonist of CB1 cannabinoid receptors. *Naunyn-Schmiedeberg's archives of pharmacology* **1995,** *352* (5), 576-579.
56. Trinka, E.; Cock, H.; Hesdorffer, D.; Rossetti, A. O.; Scheffer, I. E.; Shinnar, S.; Shorvon, S.; Lowenstein, D. H., A definition and classification of status epilepticus--Report of the ILAE Task Force on Classification of Status Epilepticus. *Epilepsia* **2015,** *56* (10), 1515-1523.
57. Colangeli, R.; Di Maio, R.; Pierucci, M.; Deidda, G.; Casarrubea, M.; Di Giovanni, G., Synergistic Action of CB1 and 5-HT2B Receptors in Preventing Pilocarpine-Induced Status Epilepticus in Rats. *Neurobiol Dis* **2019**.
58. Di Maio, R.; Cannon, J. R.; Greenamyre, J. T., Post-status epilepticus treatment with the cannabinoid agonist WIN 55,212-2 prevents chronic epileptic hippocampal damage in rats. *Neurobiol Dis* **2015,** *73*, 356-365.
59. Shubina, L.; Aliev, R.; Kitchigina, V., Attenuation of kainic acid-induced status epilepticus by inhibition of endocannabinoid transport and degradation in guinea pigs. *Epilepsy Res* **2015,** *111*, 33-44.
60. Shubina, L.; Aliev, R.; Kitchigina, V., Endocannabinoid-dependent protection against kainic acid-induced long-term alteration of brain oscillations in guinea pigs. *Brain Res* **2017,** *1661*, 1-14.
61. Di Maio, R.; Colangeli, R.; Di Giovanni, G., WIN 55,212-2 Reverted Pilocarpine-Induced Status Epilepticus Early Changes of the Interaction among 5-HT(2C)/NMDA/CB(1) Receptors in the Rat Hippocampus. *ACS chemical neuroscience* **2019,** *10* (7), 3296-3306.
62. Pecorelli, A.; Belmonte, G.; Meloni, I.; Cervellati, F.; Gardi, C.; Sticozzi, C.; De Felice, C.; Signorini, C.; Cortelazzo, A.; Leoncini, S.; et al., Alteration of serum lipid profile, SRB1 loss, and impaired Nrf2 activation in CDKL5 disorder. *Free radical biology & medicine* **2015,** *86*, 156-165.
63. Naidoo, V.; Nikas, S. P.; Karanian, D. A.; Hwang, J.; Zhao, J.; Wood, J. T.; Alapafuja, S. O.; Vadivel, S. K.; Butler, D.; Makriyannis, A.; et al., A new generation fatty acid amide hydrolase inhibitor protects against kainate-induced excitotoxicity. *J Mol Neurosci* **2011,** *43* (3), 493-502.

64. Mikheeva, I. B.; Shubina, L.; Matveeva, N.; Pavlik, L. L.; Kitchigina, V. F., Fatty acid amide hydrolase inhibitor URB597 may protect against kainic acid–induced damage to hippocampal neurons: Dependence on the degree of injury. *Epilepsy Research* **2017,** *137*, 84-94.
65. Naidoo, V.; Karanian, D. A.; Vadivel, S. K.; Locklear, J. R.; Wood, J. T.; Nasr, M.; Quizon, P. M.; Graves, E. E.; Shukla, V.; Makriyannis, A.; et al., Equipotent inhibition of fatty acid amide hydrolase and monoacylglycerol lipase - dual targets of the endocannabinoid system to protect against seizure pathology. *Neurotherapeutics* **2012,** *9* (4), 801-813.
66. Sheldrick, G. M., A short history of SHELX. *Acta Crystallogr A* **2008,** *64*, 112-122.
67. Sheldrick, G. M., Crystal structure refinement with SHELXL. *Acta Crystallographica Section C-Structural Chemistry* **2015,** *71*, 3-8.
68. Harder, E.; Damm, W.; Maple, J.; Wu, C.; Reboul, M.; Xiang, J. Y.; Wang, L.; Lupyan, D.; Dahlgren, M. K.; Knight, J. L.; et al., OPLS3: A Force Field Providing Broad Coverage of Drug-like Small Molecules and Proteins. *J Chem Theory Comput* **2016,** *12* (1), 281-296.
69. Still, W. C.; Tempczyk, A.; Hawley, R. C.; Hendrickson, T., Semianalytical Treatment of Solvation for Molecular Mechanics and Dynamics. *J. Am. Chem. Soc.* **1990,** *112* (16), 6127-6129.
70. Gasser, A.; Brogi, S.; Urayama, K.; Nishi, T.; Kurose, H.; Tafi, A.; Ribeiro, N.; Desaubry, L.; Nebigil, C. G., Discovery and cardioprotective effects of the first non-Peptide agonists of the G protein-coupled prokineticin receptor-1. *PloS one* **2015,** *10* (4), e0121027.
71. Chemi, G.; Gemma, S.; Campiani, G.; Brogi, S.; Butini, S.; Brindisi, M., Computational Tool for Fast in silico Evaluation of hERG K(+) Channel Affinity. *Front Chem* **2017,** *5*, 7.
72. Sirous, H.; Chemi, G.; Gemma, S.; Butini, S.; Debyser, Z.; Christ, F.; Saghaie, L.; Brogi, S.; Fassihi, A.; Campiani, G.; et al., Identification of Novel 3-Hydroxy-pyran-4-One Derivatives as Potent HIV-1 Integrase Inhibitors Using in silico Structure-Based Combinatorial Library Design Approach. *Front Chem* **2019,** *7*, 574.
73. Mileni, M.; Garfunkle, J.; Ezzili, C.; Cravatt, B. F.; Stevens, R. C.; Boger, D. L., Fluoride-mediated capture of a noncovalent bound state of a reversible covalent enzyme inhibitor: X-ray crystallographic analysis of an exceptionally potent alpha-ketoheterocycle inhibitor of fatty acid amide hydrolase. *J Am Chem Soc* **2011,** *133* (11), 4092-4100.
74. Brogi, S.; Fiorillo, A.; Chemi, G.; Butini, S.; Lalle, M.; Ilari, A.; Gemma, S.; Campiani, G., Structural characterization of Giardia duodenalis thioredoxin reductase (gTrxR) and computational analysis of its interaction with NBDHEX. *Eur J Med Chem* **2017,** *135*, 479-490.
75. Brogi, S.; Ramunno, A.; Savi, L.; Chemi, G.; Alfano, G.; Pecorelli, A.; Pambianchi, E.; Galatello, P.; Compagnoni, G.; Focher, F.; et al., First dual AK/GSK-3beta inhibitors endowed with antioxidant properties as multifunctional, potential neuroprotective agents. *Eur J Med Chem* **2017,** *138*, 438-457.
76. Brindisi, M.; Senger, J.; Cavella, C.; Grillo, A.; Chemi, G.; Gemma, S.; Cucinella, D. M.; Lamponi, S.; Sarno, F.; Iside, C.; et al., Novel spiroindoline HDAC inhibitors: Synthesis, molecular modelling and biological studies. *Eur J Med Chem* **2018,** *157*, 127-138.
77. Zaccagnini, L.; Brogi, S.; Brindisi, M.; Gemma, S.; Chemi, G.; Legname, G.; Campiani, G.; Butini, S., Identification of novel fluorescent probes preventing PrP(Sc) replication in prion diseases. *Eur J Med Chem* **2017,** *127*, 859-873.
78. Gattinoni, S.; De Simone, C.; Dallavalle, S.; Fezza, F.; Nannei, R.; Amadio, D.; Minetti, P.; Quattrociocchi, G.; Caprioli, A.; Borsini, F.; et al., Enol carbamates as inhibitors of fatty acid amide hydrolase (FAAH) endowed with high selectivity for FAAH over the other targets of the endocannabinoid system. *ChemMedChem* **2010,** *5* (3), 357-360.

79. Lamponi, S.; Aloisi, A. M.; Bonechi, C.; Consumi, M.; Donati, A.; Leone, G.; Rossi, C.; Tamasi, G.; Ghiandai, L.; Ferrini, E.; et al., Evaluation of in vitro cell and blood compatibility and in vivo analgesic activity of plant-derived dietary supplements. *Journal of integrative medicine* **2019,** *17* (3), 213-220.
80. D'Elia, P.; De Matteis, F.; Dragoni, S.; Shah, A.; Sgaragli, G.; Valoti, M., DP7, a novel dihydropyridine multidrug resistance reverter, shows only weak inhibitory activity on human CYP3A enzyme(s). *Eur J Pharmacol* **2009,** *614* (1-3), 7-13.
81. Williamson, B.; Wilson, C.; Dagnell, G.; Riley, R. J., Harmonised high throughput microsomal stability assay. *Journal of pharmacological and toxicological methods* **2017,** *84*, 31-36.
82. Canella, R.; Benedusi, M.; Martini, M.; Cervellati, F.; Cavicchio, C.; Valacchi, G., Role of Nrf2 in preventing oxidative stress induced chloride current alteration in human lung cells. *Journal of cellular physiology* **2018,** *233* (8), 6018-6027.
83. Saponara, S.; Ferrara, A.; Gorelli, B.; Shah, A.; Kawase, M.; Motohashi, N.; Molnar, J.; Sgaragli, G.; Fusi, F., 3,5-dibenzoyl-4-(3-phenoxyphenyl)-1,4-dihydro-2,6-dimethylpyridine (DP7): a new multidrug resistance inhibitor devoid of effects on Langendorff-perfused rat heart. *Eur J Pharmacol* **2007,** *563* (1-3), 160-163.
84. Ferrara, A.; Fusi, F.; Gorelli, B.; Sgaragli, G.; Saponara, S., Effects of freeze-dried red wine on cardiac function and ECG of the Langendorff-perfused rat heart. *Canadian journal of physiology and pharmacology* **2014,** *92* (2), 171-174.
85. Pessina, F.; Gamberucci, A.; Chen, J.; Liu, B.; Vangheluwe, P.; Gorelli, B.; Lorenzini, S.; Spiga, O.; Trezza, A.; Sgaragli, G.; Saponara, S., Negative chronotropism, positive inotropism and lusitropism of 3,5-di-t-butyl-4-hydroxyanisole (DTBHA) on rat heart preparations occur through reduction of RyR2 Ca(2+) leak. *Biochem Pharmacol* **2018,** *155*, 434-443.
86. Kmecova, J.; Klimas, J., Heart rate correction of the QT duration in rats. *Eur J Pharmacol* **2010,** *641* (2-3), 187-192.
87. Horowitz, M. P.; Milanese, C.; Di Maio, R.; Hu, X.; Montero, L. M.; Sanders, L. H.; Tapias, V.; Sepe, S.; van Cappellen, W. A.; Burton, et al., Single-cell redox imaging demonstrates a distinctive response of dopaminergic neurons to oxidative insults. *Antioxidants & redox signaling* **2011,** *15* (4), 855-871.
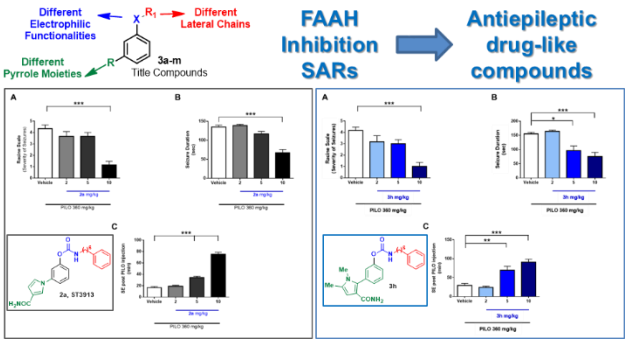
SYNOPSIS TOC